WILEY

Progress in Contactless 3D Printing and 2D Material Integration for Next-Generation Electrochemical Sensing Applications

Arshid Numan[1,2] | Lijie Li[3] | Salem AlFaify[4] | Muhammad Sheraz Ahmad[5] | Syam Krishnan[6] | Mohammad Khalid[7,8,9]

[1]Sunway Center for Electrochemical Energy Storage and Sustainable Technology, Faculty of Engineering and Technology, Sunway University, Petaling Jaya, Selangor, Malaysia | [2]Department of Applied Physics, Saveetha School of Engineering, Saveetha University (SIMATS), Chennai, India | [3]Faculty of Science and Engineering, Swansea University, Swansea, UK | [4]Advanced Functional Materials and Optoelectronics Laboratory (AFMOL), Department of Physics, College of Science, King Khalid University, Abha, Saudi Arabia | [5]Center for Environmental Sustainability and Human Health, Ming Chi University of Technology, New Taipei City, Taiwan | [6]Faculty of Engineering and Information Technology, The University of Melbourne, Melbourne, Victoria, Australia | [7]Materials and Manufacturing Research Group, James Watt School of Engineering, University of Glasgow, Glasgow, UK | [8]Faculty of Engineering, Manipal University Jaipur, Jaipur, Rajasthan, India | [9]Centre for Research Impact and Outcome, Chitkara University, Punjab, India

Correspondence: Arshid Numan (numana@sunway.edu.my) | Mohammad Khalid (mohammad.khalid@glasgow.ac.uk)

ABSTRACT

The convergence of two-dimensional (2D) nanomaterials and additive manufacturing has emerged as a transformative frontier in materials science and advanced fabrication techniques. This review systematically examines the integration of 2D materials, such as graphene, transition metal dichalcogenides, and MXenes, with 3D printing technologies, highlighting their synergistic potential in functional applications. We assessed the structural, electronic, optical, and mechanical properties of 2D materials that render them ideal for engineered inks, along with key three-dimensional (3D) printing approaches (inkjet, extrusion, and stereolithography) optimized for processing these nanomaterials. Critical challenges in ink design, including rheological control, interfacial engineering, and parameter optimization, were analyzed to bridge synthesis strategies with scalable fabrication. State-of-the-art applications in energy storage, flexible electronics, sensing, and high-performance composites have demonstrated the versatility of 3D-printed 2D architectures. Emerging opportunities in multimaterial printing, algorithmic-driven manufacturing, and sustainable production are outlined to address the current limitations in resolution, scalability, and functional integration. By integrating the progress and prospects across disciplines, this review provides a roadmap for the advancement of 2D material-enabled 3D printing in next-generation technologies.

1 | Introduction

The advent of electronic sensors in the mid-twentieth century marked a major technological shift, enabling the detection and quantification of diverse chemical and biological analytes [1].

Among these, electrochemical sensors have gained particular prominence because of their high sensitivity, selectivity, and precision, which make them indispensable across multiple sectors. Their use spans environmental monitoring, product quality assurance, and clinical diagnostics, where rapid and reliable

detection is essential for decision-making and safety [2]. The operating principle of these devices relies on electrochemical reactions that generate measurable electrical signals in response to target analytes, thereby allowing sensitive and specific quantification [3]. Furthermore, ongoing advancements in sensor miniaturization are creating new opportunities for portable and mobile applications, expanding their accessibility and practical utility in real-world settings [4, 5].

The evolution of electronics from rigid to flexible architectures has further accelerated the adoption of electrochemical sensors, particularly within the expanding framework of the Internet of Things (IoT). By integrating low-cost, ubiquitous sensors into connected systems, IoT technologies are paving the way for personalized and precision medicine, wherein wearable devices can continuously track key health indicators [6, 7]. This transition from manual, labor-intensive methods to automated, sensor-driven systems over the past five decades has reshaped daily life and established new standards in healthcare and beyond [8].

A particularly impactful outcome of these advances is the development of point-of-care (POC) technologies. Electrochemical sensors are central to these systems, which are characterized by their compact design, user-friendliness, multifunctionality, and ability to deliver rapid diagnostic results [9, 10]. Their deployment extends beyond traditional clinical environments, supporting in-home testing solutions that accelerate diagnosis, improve access to care, and enhance patient satisfaction by enabling more immediate treatment decisions [11].

However, similar to other technologies, electrochemical sensors have some drawbacks. Electrochemical sensors, particularly traditional ones, suffer from several drawbacks, including low selectivity, sensitivity, and stability [12]. Such limitations are attributed to interference from other ions and molecules in the sample or the high sensitivity of the sensing electrode, which may cause faster degradation of the sensor [13]. Furthermore, common electrochemical sensors exhibit high-temperature selectivity, low operating temperatures, and high energy consumption, which are often undesirable for portable and remote sensing applications [14]. Similarly, classic electrochemical sensors are highly susceptible to interference from other species and sample matrices, and the results obtained are often inaccurate or inconclusive [15]. Second, traditional electrochemical sensors have low sensitivity to low analyte concentrations [16]. The first significant drawback is the non-selectivity of the analytes, which is a major disadvantage of traditional electrochemical sensors because they do not allow the detection of specific targets [17, 18]. The materials used for constructing electrochemical sensors are usually thin and delicate; hence, they may demagnetize over time, resulting in drift and loss of sensitivity [19, 20]. Furthermore, the accumulation of foul materials or the blocking of a section of the electrodes impairs the function of the sensor [21]. Finally, traditional electrochemical sensors are relatively complicated and costly to fabricate and synthesize, which may restrict their application in certain areas [22, 23].

Conventional electrochemical sensors remain widely used due to their low cost and ease of operation, yet challenges related to

selectivity, surface fouling, miniaturization, and system integration limit their broader applicability. Recent advances in three-dimensional (3D) printing provide promising solutions to these constraints by enabling rapid, cost-effective, and customizable fabrication of complex architectures, such as porous electrodes and microfluidic channels [24]. These design possibilities not only reduce the prototyping time and simplify device assembly, but also address long-standing limitations without sacrificing accessibility. Moreover, 3D printing allows the fabrication of intricate micro- and nanoscale features that can significantly improve sensor performance [25]. The ability to construct multimaterial structures that seamlessly integrate electronic and electrochemical components further expands the functional versatility of electrochemical sensors, thereby opening new opportunities for high-performance and application-specific designs [26].
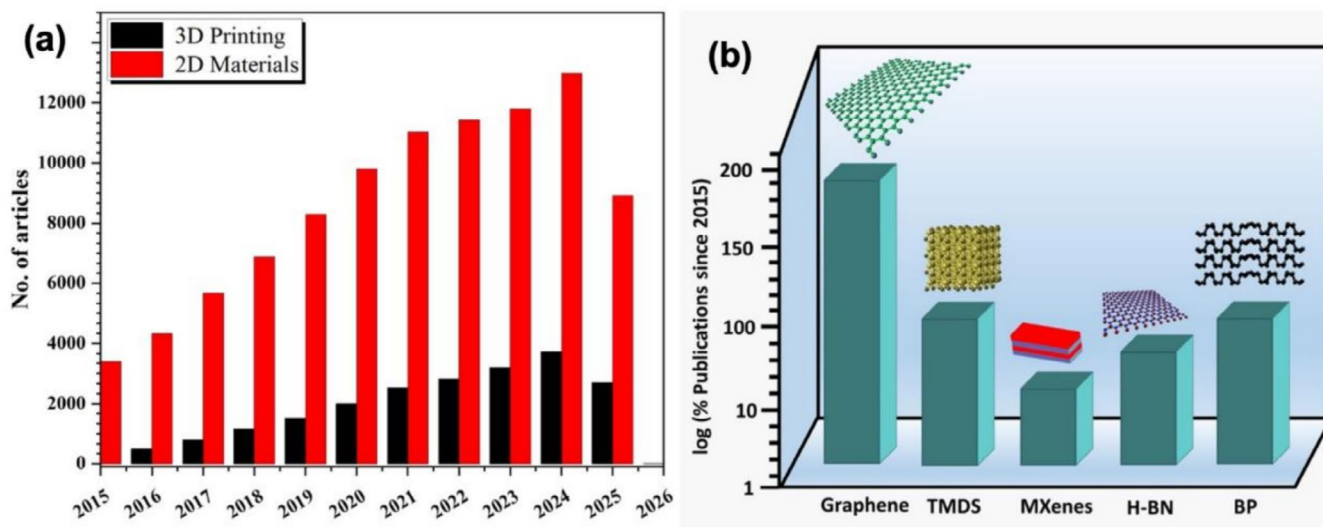
Another important advantage of 3D printing in electrochemical sensor fabrication is its capacity to significantly reduce production costs while enhancing manufacturing efficiency [27]. Conventional sensor manufacturing is often time-consuming and expensive, whereas 3D printing enables rapid and cost-effective large-scale production, facilitating iterative design improvements and optimization [28]. This flexibility not only shortens development timelines but also lowers overall expenses for both researchers and manufacturers. Reflecting its growing impact, market reports estimate that the global 3D printing industry will exceed USD 40 billion by 2024, with an annual growth rate of approximately 30%, driven by advances in materials, hardware, and process control technologies [29]. However, despite these benefits, challenges persist. In particular, limitations in printing precision and material control can compromise sensor reproducibility and accuracy, resulting in variability in performance and sensitivity [30, 31].

One way to overcome these limitations is to incorporate 2D materials into 3D printing [32]. The advancement of sensor technologies depends on 2D materials, including graphene, MXenes, nitrides, phosphorene, and transition metal dichalcogenides, because of their unique electrical, thermal, and mechanical properties. The development of smart devices, diagnostic tools, and industrial systems depends on aerospace applications, thermal and digital sensing, real-time health monitoring, environmental monitoring, and high-sensitivity detection (Figure 1).

One of the benefits of incorporating 2D materials into 3D-printed electrochemical sensors is their high surface area-to-volume ratio. This allows the incorporation of a larger quantity of active sensing materials into the sensor, thereby enhancing the sensitivity of the system [33]. Their intrinsic properties, including high electron mobility and chemical stability, further contribute to their superior selectivity in electrochemical detection [34–36]. Beyond their material attributes, 3D printing facilitates the precise design of intricate sensing architectures, allowing sensor geometries to be optimized for specific applications and enabling the integration of multiple sensing components into a single platform [37–39]. This fabrication approach also supports the layering of 2D materials with diverse substrates, resulting in sensors that are not only highly sensitive but also versatile across a broad range of analytes

FIGURE 1 | Diverse applications of 2D materials in sensors and their advancements.

[40]. Consequently, the synergy between 2D materials and 3D printing provides a powerful route for developing next-generation electrochemical sensors with enhanced sensitivity, flexibility, and multifunctionality. Over the past decade, this synergy has driven a sharp increase in research activity, as reflected by the exponential increase in publications on 3D-printed devices incorporating 2D materials (Figure 2a). Among these, graphene, transition metal dichalcogenides (TMDs), and black phosphorus (BP) have emerged as the most extensively investigated systems (Figure 2b), highlighting the growing scientific and technological interest in exploiting the complementary advantages of 2D nanomaterials and additive manufacturing [32]. Despite these advances, challenges remain in optimizing ink formulations, enhancing the conductivity of additives, and scaling fabrication methods. By addressing both the opportunities and challenges associated with these developments, this review highlights the potential of printed electrochemical sensors to drive innovations across multiple fields.

2 | Two-Dimensional Materials and Their Electrochemical Applications

2D materials have emerged as transformative platforms for electrochemical applications due to their unique structural and physicochemical properties. Unlike conventional solid-state technologies, which face challenges such as short-channel effects and high contact resistance during miniaturization [41]. 2D material-based electrochemical sensors offer superior sensitivity, selectivity, and scalability [42]. Since the isolation of graphene in 2004, research on 2D materials has expanded rapidly, with applications ranging from protective coatings to biochemical sensing [43]. Defined as atomically thin materials spanning a few atomic layers to several hundred nanometers [44], 2D systems have become highly attractive due to their large surface areas, high carrier mobility, tunable surface chemistry, and shape adaptability. These attributes make them versatile platforms for optoelectronics, catalysis, energy storage, and sensing applications [45, 46]. Consequently, 2D materials have emerged as promising candidates for modified working electrodes in electrochemical devices [47]. Their electrochemical performance is strongly dictated by their structural characteristics, including layer number, size, morphology, defects, doping, grain boundaries, and phase, which in turn govern their electronic structures and device-level functionality [48–50].

Systematic studies have confirmed that tailoring defects, doping, and layer thickness enables precise tuning of electron-transfer kinetics and sensor sensitivity. For example, in graphene, the controlled introduction of vacancy defects via ion irradiation or electrochemical bromination enhances electron transfer rates (k^0) until an optimal defect density (~ 1–2×10^{12} cm^{-2}) is reached, after which conductivity rapidly deteriorates [51, 52]. Similarly,

FIGURE 2 | Evolution and intersection of 3D printing and 2D materials based on a Web of Science bibliographic search. (a) Annual publication count on the integration of 3D printing and 2D materials. (b) Publication count by type of 2D material integrated with 3D printing technology [32].

the electrochemical detection of neurotransmitters, such as dopamine and serotonin, improves linearly with increasing point-defect density until sp^2 amorphization occurs, whereas line defects contribute minimally [53, 54]. Moreover, the addition of graphene layers enhances the density of states and accelerates electron transfer, and multilayer regions achieve reversible kinetics regardless of defect content [55]. Vertical transport is further improved by confining defects to an upper sacrificial layer in bilayer stacks [56].

Other 2D materials display contrasting behaviors. For instance, in MoS_2, each additional layer suppresses hydrogen evolution exchange currents due to the interlayer hopping barrier (0.119 V), making monolayer or bilayer flakes most efficient for catalysis [57]. Within these flakes, sulfur vacancies act as dominant active sites, enhancing local k^0 by up to fourfold [58, 59]. Heteroatom doping offers further tuning of work function and adsorption chemistry; for example, N-doped graphene (0.11–1.35 at. %) accelerates direct electron transfer in enzyme-based biosensors and significantly lowers detection limits for glucose and H_2O_2 to 0.01 mM, while graphitic-N specifically enhances acetaminophen sensing [60, 61]. Furthermore, co-doping strategies, such as N, S-doping, synergistically redistribute charge density, leading to superior dopamine sensing compared to single-doped or pristine graphene [62]. Therefore, achieving peak biosensor performance necessitates a careful match between the material structure (defect density, layer count, dopant type/concentration) and the required electron transfer kinetics. Studies that correlate structural characterization (e.g., Raman spectroscopy) with quantitative kinetic metrics (k^0, j_0) and sensing performance provide the most reliable blueprint for transducer design.

In addition to defects and doping, grain boundary engineering plays a pivotal role in enhancing charge transport. Reduced boundary densities improve carrier mobility and minimize scattering, whereas large, compositionally uniform single crystals are essential for device-grade reproducibility [63]. The vast and growing library of 2D materials, including TMDs, MXenes, and layered oxides, requires coherent classification to enable fair comparisons and guide future research (Figure 3) [64]. The following section reviews these key classes, focusing on the structural features that enhance their electrochemical efficacy.

2.1 | Graphene

Graphene, a 2D monolayer of sp^2-bonded carbon atoms arranged in a hexagonal lattice, has emerged as the cornerstone of modern materials science since its isolation in 2004 [65]. Owing to its exceptional electronic properties, including ultrahigh charge carrier mobility ($> 200000\,cm^2\,V^{-1}\,s^{-1}$), zero-effective-mass Dirac fermions, and ballistic transport over the micrometer scale at room temperature, atomically thin materials have revolutionized research in nanoelectronics, energy storage, and sensing technologies [66]. Its unique electronic structure, combined with its unparalleled mechanical strength (~130 GPa), optical transparency (97.7% per layer), and large specific surface area ($2630\,m^2\,g^{-1}$), makes graphene a transformative platform for next-generation devices [67]. In energy storage systems, graphene's high electrical conductivity ($10^6\,S\,m^{-1}$) and surface-dominated chemistry enhance charge transfer kinetics in supercapacitors and battery electrodes, while its mechanical flexibility enables robust and lightweight architectures [66]. For sensor technologies, the sensitivity of graphene to local electrical perturbations (detecting single-molecule adsorption events) and tunable surface chemistry via functionalized derivatives (e.g., reduced graphene oxide (rGO) and nitrogen-doped graphene) enable ultrasensitive detection of chemical and biological analytes [68]. Recent advances in scalable synthesis techniques, such as chemical vapor deposition (CVD) and solution-based exfoliation, have mitigated the early challenges related to defect density and conductivity, although inherent trade-offs between processability and performance remain for exfoliated materials [69]. The incorporation of graphene into hybrid systems, particularly with MXenes or conducting polymers, has further broadened its application scope, enabling progress in flexible electronics and integrated energy storage–sensing platforms. As the field transitions from fundamental studies to

2D MAGNETIC MATERIALS
FePS$_3$, NiPS$_3$, MnPS$_3$, FePS$_3$, FePSe$_3$, GeSe, MnSe, MnSe$_2$, FeS, FeSe, FeTe$_{1-x}$Se$_x$, FeTe, FeTe$_2$, Fe$_3$TaS$_2$, Cr$_5$Te$_8$, Ta$_3$FeS$_6$, Bi$_2$O$_2$Se, Fe$_3$GeTe$_2$, Na$_{0.5}$Bi$_{4.5}$Ti$_4$O$_{15}$, VSe$_2$, LiNbO$_3$, LiTaO$_3$, Another family of 2D magnetic materials

2D FERROELECTRIC & MULTIFERROIC MATERIALS
CuInP$_2$S$_6$, SnTe, GeSe, SnSe, GeS, SnS, α-In$_2$Se$_3$, In$_2$Se$_3$, WTe$_2$, Fe-doped In$_2$Se$_3$, β'-2Hα-In$_2$Se$_3$, BA$_2$PbCl$_4$, d1T-MoTe$_2$, Bi$_2$O$_2$Se, etc.

2D COMPLEX-METALLIC DICHALCOGENIDE MATERIALS
NbS$_2$, TiS$_2$, NiSe$_2$, NiTe$_2$, NiSe$_{2-x}$Te$_x$, etc.

2D SUPERCONDUCTING MATERIALS
MoTe$_2$, NbSe$_2$, NbTe$_2$, WTe$_2$, Bi$_2$Sr$_2$CaCu$_2$O$_{8-x}$, ZrNCl, etc.

2D CARBON FAMILY
Graphite, Graphene, Graphene Oxide, Graphane, Graphyne, Graphyne, Graphdiyne, Fluorographene

2D SEMIMETAL MATERIALS WITH POLYMORPHS
1T'-WS$_2$, 1T'-WSe$_2$, 1T'-MoS$_2$, 1T'-MoSe$_2$, 1T'-WS$_2$xSe$_{2(1-x)}$, 1T'-MoS$_2$xSe$_{2(1-x)}$, (C$_{2h}$, D$_{3h}$, D$_{3d}$)-InSe, T-Mo$_2$C, (2H, 1T, 1T")-CrS$_2$, (1H, 1T, 1T")-MoTe$_2$, v1H-Mo$_2$Te$_6$, (1H, 2H, 1T, 2Ha, 4Hb, 6R, 2Ha)-TaS$_2$, 1T-TaSe$_2$, 1T"-WTe$_2$, 1T-2H MoS$_2$, 1T-PtSe$_2$, 1T-MoTe$_2$, 2H-NbS$_2$, tr-BeN$_4$, Another polymorphism-based TMDs

2D PEROVSKITE MATERIALS
LaNb$_2$O$_7$, (Ca,Sr)$_2$Nb$_3$O$_{10}$, Ca$_2$Nb$_3$O$_{10}$, Ca$_2$NaNb$_4$O$_{13}$, Ca$_2$Na$_2$Nb$_5$O$_{16}$, Ca$_2$Na$_2$Nb$_5$O$_{16}$, Ca$_2$Na$_3$Nb$_6$O$_{19}$, Ti$_{1.87}$O$_2$, Ti$_{0.91}$O$_2$, Ti$_2$NbO$_7$, TiNBO$_5$, Ti$_5$NbO$_{14}$, BiTiO$_2$, Ca$_2$Nb$_3$O$_{10}$, Ca$_2$NaNb$_4$O$_{13}$, Ca$_2$Na$_2$Nb$_5$O$_{16}$, Ca$_2$Na$_3$Nb$_6$O$_{19}$, Ca$_{12}$Ta$_2$TiO$_{10}$, Ca$_2$Ta$_3$O$_{10}$, Sr$_2$Ta$_3$O$_{10}$, Sr$_2$Nb$_3$O$_{10}$, Nb$_3$O$_8$, La$_{0.95}$Nb$_2$O$_7$, La$_{0.9}$Eu$_{0.05}$Nb$_2$O$_7$, Eu$_{0.56}$Ta$_2$O$_7$, BSCCO, BaZrS$_3$, (C$_6$H$_5$NH$_3$)$_2$PbX$_4$ (X=Cl, Br, I), etc.

2D SEMICONDUCTING DICHALCOGENIDE MATERIALS
NiTe$_2$, CoTe$_2$, ReS$_2$, PtTe$_2$, ZrS$_2$, ZrSe$_2$, HfSe$_2$, SnSe$_2$, PtSe$_2$, MoS$_2$, MoSe$_2$, SnP$_3$, SnS, SnS$_2$, SnSe$_2$, GaSe, GaTe, Ga$_2$S$_3$, Bi$_2$Se$_3$, Bi$_2$Te$_3$, Bi$_2$S$_3$, Sb$_2$Te$_3$, Sb$_2$Se$_3$, Sb$_2$S$_3$, GeP, SiAs, GeAs, NbS$_2$, InSe, In$_2$Se$_3$, WS$_2$, WSe$_2$, PdSe$_2$, PtS$_2$, PdS$_2$

2D CHROME-BASED DICHALCOGENIDE MATERIALS
CrI$_3$, CrCl$_3$, Cr$_2$Ge$_2$Te$_6$, Ce$_2$S$_3$, CrSe, CrCX (C=S, Se,Te, X=Cl, Br, I), CrOX (X=Cl, Br), CrTe$_2$, Cr$_5$Te$_8$, Cr$_2$Ge$_2$Te$_6$, Cr$_2$Si$_2$Te$_6$, CrGeTe$_3$, CrSe$_2$, CrSe, Cr$_2$Se$_3$, etc.

2D MONOELEMENT MATERIALS
Black-White-Red Phosphorous, Black Phosphorene, Tellurene, Borophene, Silicene, Germanene, Stanene, Arsenene, Antimonene, Bismuthene, Plumbene, Gallenene, Selenene, Co, Ag nanoplates, AuSSs, Pd NSs, Ru NSs, Rh NSs, etc.

OTHER 2D MATERIALS
Boron Phosphide, MoSi$_2$N$_4$, WSi$_2$N$_4$, MXenes, hBN, BCN, Ta$_2$NiS$_5$, Ta$_2$NiSe$_5$, Ta$_2$NiSe$_7$, GaAs, AlGaAs, VS$_2$, MoSi$_2$N$_4$, Pt$_2$HgSe$_3$, PdPSe, PtSSe, As$_2$S$_3$, Zn-TCCP, MOF nanosheets, etc.

2D HYDROXIDE MATERIALS
Cu(OH)$_2$, Ni(OH)$_2$, Mg(OH)$_2$, Eu(OH)$_3$, etc.

2D OXIDE MATERIALS
ZnO, Mica, MoO$_3$, WO$_3$, CuO, Cu$_2$O, TiO$_2$, TeO$_2$, MnO$_2$, V$_2$O$_5$, TaO$_3$, Ta$_2$O$_5$, ZrO$_2$, RuO$_2$, SrRuO$_3$, Ga$_2$O$_3$, Nb$_2$O$_5$, RuO$_2$, Sb$_2$O$_3$, VOI$_2$, VOBr$_2$, VOCl$_2$, VOF$_2$, TiOI$_2$, CrOI$_2$, Bi$_2$MoO$_6$, etc.

FIGURE 3 | Overview of the current state of available 2D representation materials [41].

application-driven engineering, graphene has emerged as a pivotal material that bridges condensed matter physics with industrial innovation, offering scalable pathways for high-efficiency energy harvesters, selective biosensors, and next-generation energy storage technologies beyond lithium-ion batteries [70]. This progression highlights the enduring role of graphene as both a testbed for quantum phenomena and a versatile material for sustainable technology development.

2.2 | Transition Metal Dichalcogenides

TMDs have emerged as promising candidates for advanced electrochemical sensing applications, offering distinctive advantages owing to their unique physicochemical properties. These 2D materials, composed of transition metal atoms (Mo, W, Ni, etc.) sandwiched between chalcogen layers (S, Se, Te, etc.), exhibit remarkable structural, electronic, and optical characteristics that enhance their sensing capabilities [71]. The exceptional surface area-to-volume ratio of TMDs, coupled with their tunable electronic properties, facilitates superior sensitivity to environmental perturbations, making them particularly effective in electrochemical detection systems [72]. By strategically functionalizing with organic molecules or metallic nanoparticles, it is possible to precisely adjust their electroconductive properties, thereby enhancing their effectiveness for particular sensing applications [73]. Extensive investigations of archetypal TMDs, notably MoS$_2$ and WS$_2$, have demonstrated their efficacy in electrical signal transduction, thereby establishing their utility in diverse sensing platforms [74]. These materials exhibit distinctive electronic characteristics, including thickness-dependent and compositionally tunable band gaps [75, 76]. Theoretical studies suggest further property optimization through strain engineering [77, 78], while the inherent piezoelectric properties of specific TMDs present opportunities for flexible sensing devices. The economic viability of commonly employed transition metals (Mo, W, Ni, etc.) compared to that of traditional sensing materials enhances the practical applicability of TMD-based sensors. Although preliminary studies have validated their potential in biomedicine, environmental monitoring, and food safety applications, systematic investigations of structure–property relatio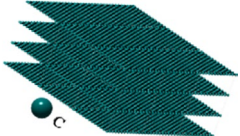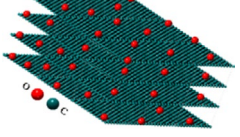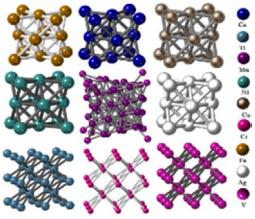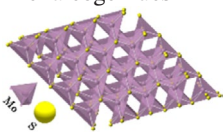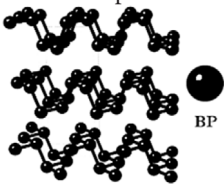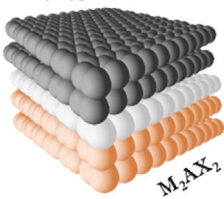nships and sensing mechanisms remain crucial for optimizing their performance and establishing their advantages over conventional sensing platforms.

2.3 | MXenes

The discovery of graphene has catalyzed the development of diverse 2D materials, including TMDs, hexagonal boron nitride (h-BN), and layered metal oxides. Among these, MXenes, a novel class of 2D transition metal carbides, carbonitrides, and nitrides, have emerged as a promising platform for electrochemical sensing applications [42]. MXenes are typically composed of early transition metals (e.g., titanium, vanadium, and niobium) bonded to carbon or nitrogen atoms in a well-ordered layered structure. Their unique two-dimensional morphology, coupled with their high specific surface area and excellent electrical conductivity, makes them highly suitable for electrochemical sensing applications. A notable advantage of MXenes is their surface hydrophilicity and the presence of tunable surface functional groups (T$_x$), such as —O, —OH, and —F, which significantly influence their surface chemistry and interactions with analytes [79]. Among various MXene compositions, Ti$_3$C$_2$T$_x$ has emerged as one of the most widely studied and utilized variants. It exhibits high electrical conductivity, a large surface area, and notable temporal stability, which are critical features for developing reliable and sensitive electrochemical sensors. These properties enable MXenes to serve as effective platforms for the detection of biomolecules, environmental pollutants and toxic compounds [80]. As research into MXenes continues to expand, their versatility and performance suggest strong potential for the next generation of high-performance electrochemical sensing technologies, offering innovative solutions to challenges in healthcare, environmental monitoring, and industrial process control. A consolidated view of 2D materials in 3D-printed electrochemical sensing, including their properties, strengths, and shortcomings, is presented in Table 1.

The properties and advantages of the two major dimensional materials are summarized in Table 1, while Table 2 presents the quantitative electrochemical sensor performance in printed or printable architectures. The selection of the best material

TABLE 1 | Summary of different 2D materials and their properties, advantages, and limitations in 3D printing of electrochemical sensors.

Material	Properties	Advantages	Limitations
Graphene	Excellent electrical conductivity, surface area, chemical stability, Low background current, Biocompatible	High sensitivity, Fast response time, Wide detection range	High production cost, Limited availability, Poor mechanical strength, Susceptible to oxidation
Graphene Oxide	High surface area, Functional groups for easy binding, Good dispersibility in solvents, enhanced electrochemical activity	Low cost, Easy functionalization, good stability in aqueous solution, Versatile fabrication methods	Reduced electrical conductivity, Prone to aggregation, Moderate sensitivity, Limited mechanical strength
Transition Metals	Good electrical conductivity	High catalytic activity	Limited to specific reactions
Dichalcogenides	Large surface area, Good mechanical flexibility, good biocompatibility, Layered structure for easy exfoliation	Chemical stability, Tailorable bandgap, High selectivity	Limited availability, Complexity in synthesis, Susceptible to oxidation, Limited charge carrier mobility
Black Phosphorus	High carrier mobility, Good optical properties, Layered structure for easy exfoliation, good biocompatibility	Wide tuneable bandgap, High sensitivity, Good mechanical flexibility	Susceptible to oxidation, Limited stability in air, Limited availability, Difficult to process
MXenes	Good electrical conductivity, High mechanical strength, Good chemical stability, good biocompatibility	Large surface area, good stability in aqueous solutions, Wide range of functionalization, Excellent electrochemical activity	Limited availability, Complex synthesis and processing, Moderate sensitivity, Limited charge carrier mobility

for a specific analyte and printing method must be determined by benchmarking sensitivity, limit of detection (LOD), and linear range.

The design of printed electrochemical sensors increasingly emphasizes sustainability and performance. To achieve this, fabrication processes should incorporate cradle-to-gate life cycle assessments and waste minimization strategies, particularly for 2D material inks and associated printing waste streams. Sustainable approaches include the use of water-based, low-toxicity formulations, implementation of closed-loop solvent recovery systems, and careful monitoring of effluents from etching and functionalization, while adopting low-temperature curing methods to reduce both energy consumption and environmental impact [90]. In the case of 3D printing for sensor fixtures, microfluidics, and tooling, waste streams typically consist of support structures, failed builds, resin wash solvents, purge materials, and particulate slurry. Best practices in the field require segregation and inventory management of these waste streams, complete curing of photopolymers prior to disposal, solvent recovery through distillation, and recycling of thermoplastics via mechanical or chemical methods. Furthermore, additive manufacturing strategies, such as minimizing support structures and employing panelization techniques, can significantly reduce scrap material. The advanced integration of web metrology

TABLE 2 | Representative sensing performance metrics of 3D-printable 2D-material-based electrochemical biosensors include the target analyte, detection technique, sensitivity, linear range, and LOD.

Class	Material/ architecture	Target	Sensitivity (units)	Linear range	LOD	Sources
Graphene	TH/rGO/ CMK-3/AuNPs nanocomposite on GCE	miR-21	NR	0.1 fM–1 pM	0.046 fM	[81]
Graphene (paper)	AuNP/RGO paper electrode	miR-21	$351.1\,\mu A \cdot mL \cdot \mu g^{-1} \cdot cm^{-2}$	0.25–$2.0\,\mu g\,mL^{-1}$ (≈ 12–96 nM)	12.0 nM	[82]
TMD (MoS$_2$)	AuNPs@MoS$_2$ nanosheets	miR-21	NR	10 fM–1 nM	0.78 fM (DPV); 0.45 fM (EIS)	[83]
TMD (MoS$_2$)	Mn-doped MoS$_2$ on porous graphene scaffold (PGS)	Dopamine (PBS)	NR	50 pM–50 μM	50 pM	[84]
MXene (Ti$_3$C$_2$T$_x$)	Ti$_3$C$_2$T$_x$ @UIO-66-NH$_2$ on GCE	Dopamine	$14.72\,\mu A\,fM^{-1}\,cm^{-2}$	1–250 fM	0.81 fM	[85]
MXene–TMD heterostructure	MXene–MoS$_2$+CHA (Thi, AuNPs)	miR-21	NR	100 fM–100 nM	26 fM	[86]
MXene–TMD (ECL)	MoS$_2$ QDs–MXene (with Au NPs lipid layer)	miRNA-135b	NR	30 fM–20 nM	10 fM	[87]
TMD–MXene	MoS$_2$ @Ti$_3$C$_2$ (heterostructure)	miR-92a-3p	NR	1–10^8 fM	0.27 fM	[88]
MXene	Ti$_3$C$_2$T$_x$ composites (examples)	Dopamine	up to $1050\,\mu A\,mM^{-1}\,cm^{-2}$ (DNA/Pd/Pt)	0.2–1000 μM	down to 30 nM	[89]

and machine vision in inline systems allows for real-time thickness control, linking feedback to viscosity, dryer power, and web tension adjustments, thereby reducing defect-driven waste. These avoided material and energy losses can then be quantified against life cycle assessment baselines, with waste per unit area tracked over time [91–93]. Finally, in the absence of supplier-provided life cycle data, sustainability can be reinforced by setting explicit environmental thresholds, such as requiring solvent recovery efficiencies above 90%, implementing volatile organic compounds (VOCs) capture systems, and ensuring documented end-of-life strategies for support materials [93, 94].

3 | Conventional Electronic Sensing Approaches for the Architecture Frameworks

Electrochemical sensors are widely employed to detect and quantify specific chemical species in various samples. These sensors function based on electrochemical reactions involving the transfer of electrons between a working electrode and a reference electrode [95]. The concentrations of the target analytes were determined by measuring the current or voltage generated during the electrochemical response. The working electrode is central to the performance of the sensor, serving as an active site for electrochemical reactions [96]. Typically, these electrodes are composed of highly conductive and chemically stable biocompatible materials, such as gold, platinum, or carbon [97, 98]. The fabrication of electrochemical sensors involves various techniques for depositing electrode materials on suitable substrates. Among these, 2D printing technologies have gained prominence due to their ability to produce functional nanomaterials. These techniques can be broadly categorized into contact (mask-based) printing and noncontact (digital or maskless) approaches [99].

3.1 | Contact Printing Methods

Contact printing techniques are particularly advantageous for large-scale sensor production owing to their high throughput, scalability, and compatibility with roll-to-roll (R2R) processing [100]. Common contact printing methods include screen printing, gravure printing, flexography, and soft lithography, all of which involve direct transfer of ink or functional materials from a patterned surface to the substrate [101]. Screen printing is of
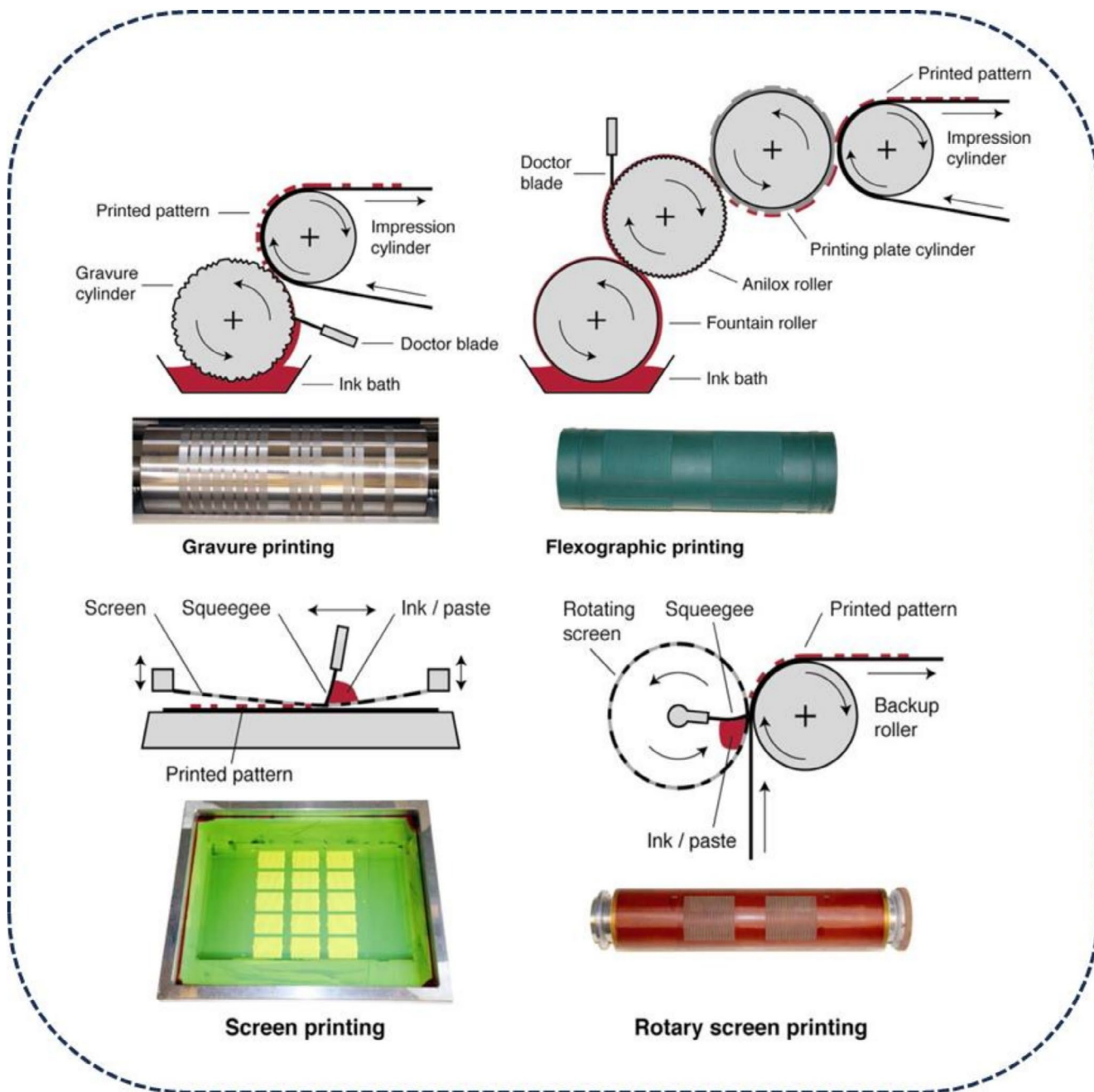
FIGURE 4 | Schematic illustration shows printing techniques using permanent printing forms, specifically gravure, flexographic, and screen printing, using either flatbed or rotary designs. Below each illustration is an image of the corresponding printing form [102].

particular interest for electrochemical sensor fabrication because of its simplicity, cost-effectiveness, and adaptability, as illustrated in Figure 4 [102].

Screen printing is a stencil-based process in which ink is transferred onto a substrate via a mesh screen (silk, synthetic fiber, or metal) using a rubber squeegee. This allows the deposition of thick layers ($> 5\,\mu m$) of functional materials, enabling robust film formation on diverse substrates, including plastics, textiles, and fibers [103]. Their high throughput, low equipment cost, and ability to reproduce identical patterns make them ideal for fabricating flexible chemicals and biosensors [104, 105]. Screen printing can be executed manually or via

automated systems, with fully automated flatbed presses achieving production rates exceeding 70 m/min while minimizing variability [106]. The critical parameters influencing print quality include the mesh count, wire diameter, and screen deflection angle [107–109].

In contrast, gravure printing, a high-speed, direct-contact technique, utilizes an engraved roller to precisely transfer ink onto substrates, with ink deposition controlled by the cell geometry (size, depth, and wall thickness) of the roller [110]. Key process variables, including printing speed, roller pressure, ink viscosity, and cell geometry, strongly influence print resolution and layer homogeneity. Although gravure printing offers high throughput

and compatibility with R2R manufacturing, its broader adoption in functional sensor fabrication has been limited by high ink consumption and setup costs [111]. Similarly, squeegee-assisted techniques facilitate the transfer of ink by pressing it through the patterned areas of a concave plate onto the substrate. This approach is well suited for flexible electronics, as it accommodates low-viscosity inks and enables fine adjustments in printed layer thickness and resolution by adjusting the shape, area, and depth of the cell [112].

Flexographic printing offers another scalable option, employing an anilox roller to regulate ink transfer from the plate to the substrate. Unlike gravure, it uses flexible rubber or elastomeric plates, which enable printing on a wide range of materials and surfaces [113, 114]. This process facilitates high-resolution patterning on a wide range of flexible substrates and benefits from halftone technology, which provides smooth and continuous lines that are not limited to dot-based resolution, as in screen and inkjet methods [115–117]. Combined with R2R production speeds of 0.2–1.5 m/s, flexography has significant potential for high-throughput fabrication of low-cost, disposable sensors [118].

Beyond these established contact printing methods, soft lithography has emerged as a powerful technique for developing highly selective biomimetic sensors via surface imprinting [119]. This technique excels in patterning electronics on curved surfaces using flexible polymeric stamps, especially when integrated with R2R processing for high-throughput production [120]. By imprinting molecular or biological species onto solid substrates, soft lithography achieves feature sizes ranging from 30 nm to 100 μm without requiring expensive materials or specialized equipment [121]. However, this process involves multiple steps, including photolithography, which can be time-consuming and require specialized training [122].

3.2 | Non-Contact/Digital Printing Methods

Non-contact digital printing methods, such as inkjet printing, laser direct writing, and aerosol printing, offer significant advantages over traditional contact-based techniques for fabricating electrochemical sensors. Unlike contact printing, these methods involve only the deposition material contacting the substrate, thereby minimizing the risk of contamination and mechanical damage to delicate substrates or pre-patterned components [101]. By eliminating the need for physical contact or masks, non-contact printing enhances the printing speed, quality, and versatility, enabling precise patterning on a wide range of substrates without applying mechanical pressure. Material deposition is controlled through nozzles or print heads, which deliver high accuracy, resolution, and multilayered deposition capabilities [100, 123]. These attributes make non-contact printing ideal for applications requiring intricate patterns and high-throughput production, as depicted in Figure 5. The ability to achieve precise, scalable, and contamination-free fabrication highlights the potential of these techniques for advancing electrochemical sensor development, offering improved performance and broader industrial applicability.

Inkjet printing technology, originally developed in the 1980s by Hewlett-Packard and Canon to provide cost-effective printing solutions for homes and offices, has since evolved into a versatile tool for advanced material fabrication [127]. Unlike thermal transfer printing, which requires direct contact between the print head, ink film, and substrate, inkjet printing is a non-contact digital technique that can precisely deposit liquids onto a wide range of substrates [128, 129]. This process relies on the ejection of microdroplets, typically through either continuous inkjet (CIJ) or drop-on-demand (DOD) mechanisms. Although CIJ, with droplet sizes of ~100 μm, is commonly used for coding and marking, DOD dominates graphic and text applications, achieving finer resolutions with droplet diameters of 20–50 μm [130, 131]. A key advantage of inkjet printing is its ability to accurately control droplet size and placement under ambient conditions, enabling high-resolution patterning with minimal material waste and reduced risk of cross-contamination. Furthermore, this technique facilitates mask-free fabrication of complex architectures, making it particularly attractive for processing thermosensitive materials, polymers, and metal oxides [129, 132]. Despite its relatively slow printing speed, which can be enhanced to ~10 m/min by incorporating additional nozzles [103], achieving high resolution remains a challenge due to the limitations imposed by droplet size. Nevertheless, the precision, flexibility, and cost-effectiveness of inkjet printing make it a powerful method for advancing sensor technology, enabling the rapid prototyping and scalable manufacturing of high-performance electrochemical devices.

Functional inks based on nanomaterials have enabled significant advances in microscale digital fabrication, particularly in aerosol jet printing (AJP). This technique has gained increasing attention owing to its high precision, efficiency, and suitability for fabricating miniaturized devices [133]. Unlike traditional inkjet printing, AJP operates through a non-contact deposition process in which the thickness of the atomized liquid is not critical, thereby eliminating the need for extensive ink adjustment. This method combines the key advantages of programmability, versatility, and resolution and can print features up to 10 μm in size, making it highly suitable for the preparation of individualized, batch-produced, and miniaturized electrochemical sensors [134, 135]. The AJP process consists of four steps: breaking the ink into tiny particles (atomization), compacting the particles (densification), aligning the particles into a stream (focusing), and finally applying the particles to the surface (deposition).

Atomization, achieved via pneumatic or ultrasonic techniques, generates a stable mist that is transported by a carrier gas to the deposition head. Because the ink does not directly contact the nozzle sidewalls, the risk of clogging is minimized, and long-term print stability is enhanced. Notably, AJP is compatible with a broad range of inks, as long as they can form aerosol droplets, which makes it a useful platform for testing and optimizing new functional ink formulations. Moreover, this method accommodates inks with viscosities ranging from 1 to 1000 cP, providing flexibility in formulation design compared to conventional inkjet systems [136–138]. These characteristics make AJP particularly well-suited for continuous deposition of conductive pathways, interconnections, and electrode structures in electrochemical devices. However, despite its growing adoption,
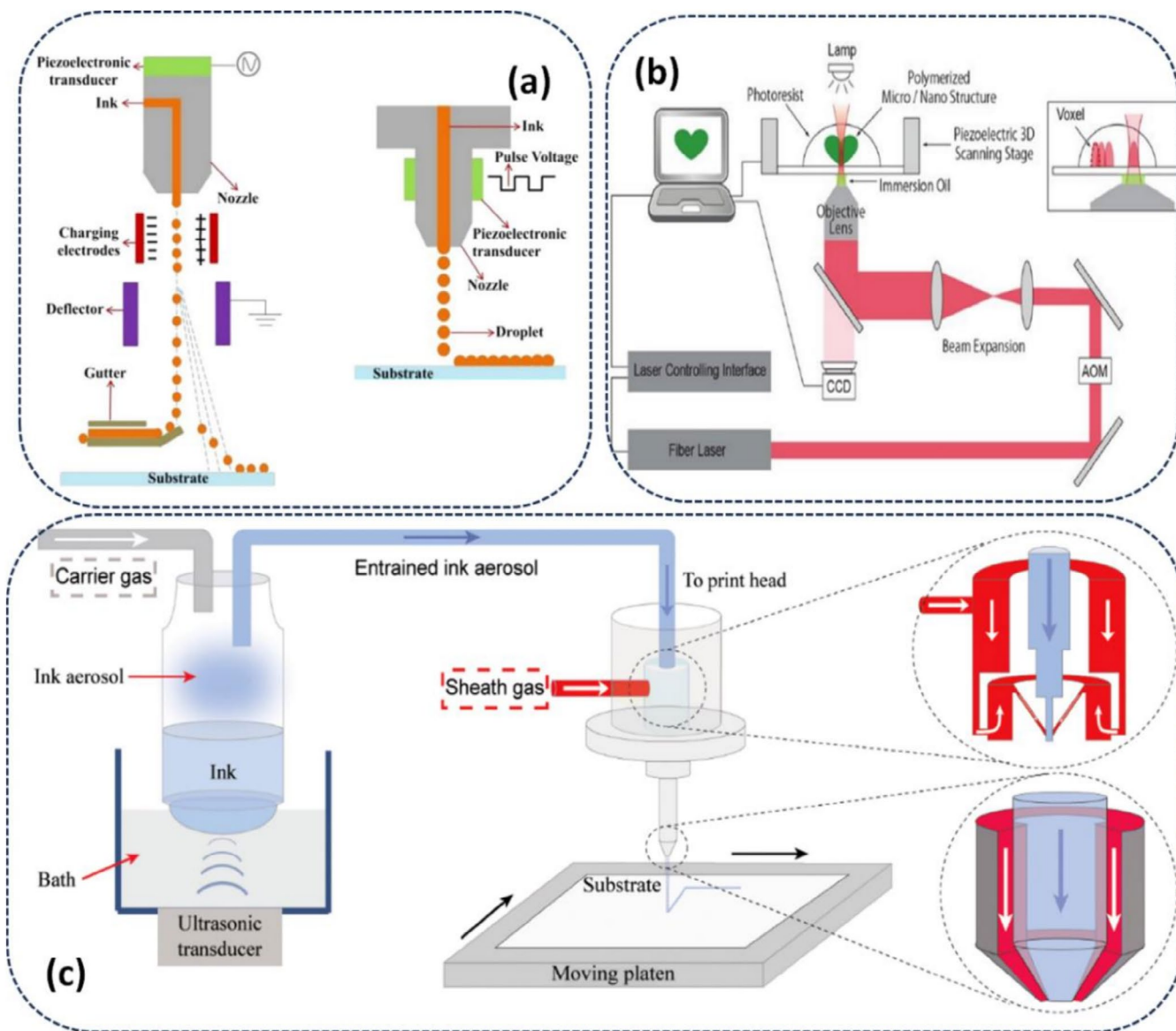
FIGURE 5 | Schematic diagrams of digital printing methods: (a) continuous inkjet printing and drop-on-demand inkjet printing [124], (b) laser direct writing [125], and (c) aerosol jet printing [126].

challenges remain in establishing optimal printing parameters across diverse inks and substrates, which continue to limit their scalability and reproducibility [100, 139].

Laser direct writing (LDW) offers another powerful approach for high-resolution micro- and nanofabrication. This enables the fabrication of precise, high-resolution patterns on two-dimensional surfaces, offering resolutions on the order of hundreds of nanometers, high writing speeds, broad coverage, and significant versatility [140]. Unlike conventional lithographic methods, LDW allows direct patterning of materials, including metals, semiconductors, polymers, and ceramics, without the need for masks or physical contact with the substrate [101]. This flexibility has made LDW an increasingly attractive technique for fabricating microstructures, supporting applications in photomask production, integrated circuits, micro-optic devices, and surface microengineering [141, 142]. Despite these advantages, LDW faces challenges when applied to sensing platforms, particularly in terms of scalability,

fabrication across diverse dimensions, and cost efficiency for highly complex structures [143]. These limitations highlight the importance of carefully selecting fabrication strategies that balance precision, cost, and application-specific requirements, with printing methods playing a decisive role in device performance.

Although advanced methods have enabled the development of 2D sensors, their limited flexibility in customization constrains their broader applications, particularly in robotic systems. In this context, 3D printing has emerged as a faster and more versatile alternative, addressing many of the inefficiencies associated with traditional manufacturing [144]. By enabling the direct integration of electrical components into custom architectures, 3D printing facilitates the design of multifunctional and application-specific sensors [145]. Beyond its technical benefits, 3D printing is increasingly recognized as a transformative technology with the potential to drive the next wave of industrial changes.

Although conventional fabrication methods have advanced electronic sensing, they remain constrained by high tooling costs, limited geometric freedom, restricted material compatibility, and slow prototyping cycles. These factors hinder innovation in multifunctional and miniaturized designs. In contrast, 3D printing provides layer-by-layer fabrication of complex architectures, seamless multi-material integration, and rapid, cost-effective prototyping. Its agility in design and on-demand production directly overcomes the limitations of traditional techniques, highlighting the need for closer examination of 3D printing principles, fabrication strategies, and their applications in sensor technologies.

4 | Unlocking the Power of 3D Printing: Transforming the Landscape of Design

Technological innovation has historically driven transformative changes in manufacturing, from mechanization during the Industrial Revolution to the current wave of digital and additive manufacturing [146]. Today, 3D printing, or additive manufacturing (AM), represents a cornerstone of the Fourth Industrial Revolution, revolutionizing biosensor manufacturing and integration by leveraging digital design and automated fabrication. This technology integrates computer-aided design with automated component evaluation, enabling the production of complex 3D structures at significantly lower costs than traditional molding techniques. Such advancements enhance global market competitiveness and drive innovation across industries [147].

Furthermore, accessibility of 3D printing has dramatically increased with the advent of low-cost desktop printers and open-source software, making it a cost-effective and versatile tool for prototyping and laboratory research [148]. This impact is particularly evident in analytical chemistry, where the utilization of 3D-printed electrochemical sensors has grown significantly. Unlike traditional approaches, 3D printing offers cost-effective fabrication while allowing the creation of customizable geometries, use of diverse materials, and seamless integration into microfluidic devices [149].

The surge in interest in 3D printing and AM reflects their recognition as disruptive technologies with the capacity to redefine the design and production of components [150]. Unlike traditional functional printing methods, such as inkjet, screen, gravure, and flexographic techniques, 3D printing enables the direct production of end-use components with unprecedented precision and customizations. Its ability to fabricate structures across multiple scales, from macro to nanoscale, has unlocked new opportunities for creating electrochemical devices with highly controlled 3D architectures [151].

As illustrated in Figure 6, a key advantage of 3D printing is its design flexibility, which allows for controlled geometries, tunable porosity, and the use of multiple precursor materials to achieve specific rigidity, size, and shape requirements. Depending on the technique employed, printed structures can range from millimeter to meter scale, with resolutions determined by the underlying process [153]. Moreover, advances in multi-material printing have unlocked the ability to manipulate materials simultaneously in space and time, yielding highly intricate, multifunctional structures that were previously unattainable through conventional manufacturing methods. These capabilities highlight the transformative potential of additive manufacturing and its expanding role in materials science, electrochemical device engineering, and broader industrial innovation [154].

The electrochemical performance of 3D-printed electrodes (3DE) is strongly influenced by microstructural defects that arise during the printing process. Defects, such as microcracks, interfacial voids, and uncontrolled porosity, impede efficient charge transport, thereby reducing both electron transfer kinetics and signal fidelity. In particular, the additive manufacturing of carbon- and graphene-based electrodes often introduces microcracks and interstitial voids as a result of solvent evaporation, particle shrinkage, and imperfect inter-road fusion during deposition. For instance, SEM analysis of inkjet-printed graphene films annealed at 150°C for 60 min revealed a network of microcracks, leading to increased sheet resistance and reduced conductivity [155]. Similar degradation phenomena are evident in fused-filament electrodes, where poor interlayer adhesion generates significant contact resistance. This manifests electrochemically as increased peak separation for outer-sphere redox probes, shifting from the theoretical 57 mV (reversible) to 90–100 mV, thereby signifying a slower apparent electron-transfer rate (ETR) and reduced sensor responsiveness [156].
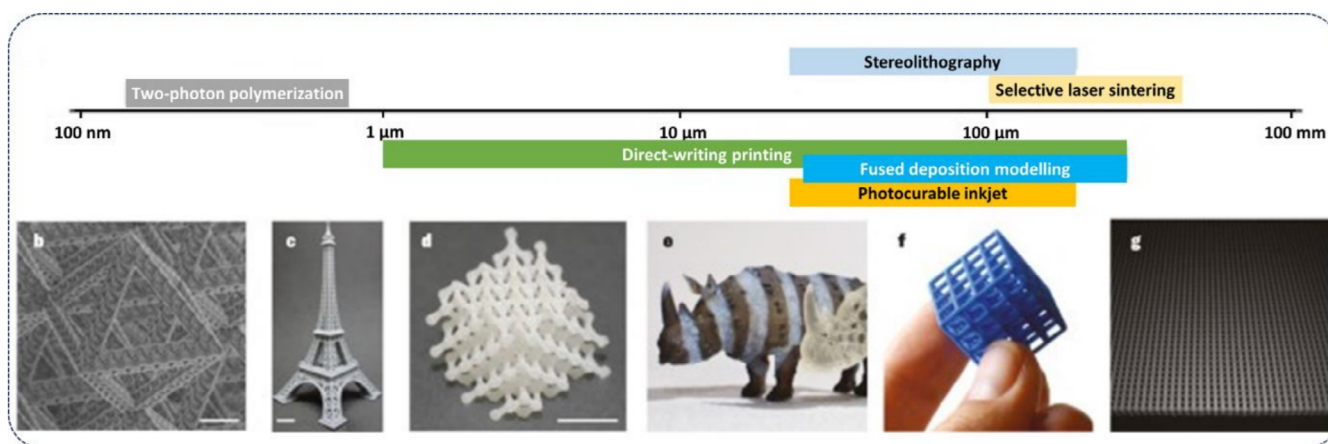
FIGURE 6 | Sizes and shapes of typical 3D-printed objects [152].

Furthermore, systematic variations in print speed demonstrate that rates exceeding $80\,mm\,s^{-1}$ disrupt conductive pathways, elevating peak separation (ΔE) and suppressing anodic currents compared to slower, well-fused prints [157].

Although porosity can enhance certain electrochemical properties, it introduces trade-offs that complicate electrode performance. For instance, increasing the void fraction of triply periodic minimal surface (TPMS) lattices from 50% to 90% enhances the electrochemically active surface area and lowers the hydrogen evolution overpotential. However, it simultaneously increases the double-layer capacitance and promotes non-uniform current distribution, destabilizing signals under high-rate operation [158]. Similarly, studies on porous carbon have shown that enlarging meso/macropores elevates areal capacitance from 200 to $350\,F\,g^{-1}$, yet this improvement is offset by broadened capacitive backgrounds at high scan rates, which obscure kinetic features and reduce signal-to-noise ratio [159].

Therefore, mitigation strategies aim to restore conductive continuity while minimizing capacitive interference. Low-temperature thermal annealing and laser sintering have proven effective in repairing microcracks and increasing inter-flake neck density, thereby reducing sheet resistance without compromising the integrity of printed geometries [155]. Additionally, post-print surface treatments, including mechanical polishing, plasma activation, or chemical functionalization, expose fresh graphitic domains that yield narrower ΔE values, resulting in sharper and less noisy voltammograms [160].

Despite significant advances, microstructural heterogeneities in 3DE continue to pose major challenges. These defects, such as microcracks that create electronic bottlenecks and uncontrolled porosity that contribute to capacitive noise, undermine electrochemical performance, even though porosity can increase the geometric surface area. Therefore, fully optimizing these architectures requires the accurate characterization of defect populations. Techniques like crack density assessment (via SEM or tomography) and pore volume quantification (e.g., using mercury intrusion porosimetry or X-ray CT) are essential for elucidating the mechanistic link between the structure and electrochemical response. The type and severity of these defects are fundamentally dictated by the printing technique. Processes such as selective laser melting (SLM), fused deposition modeling (FDM), digital light processing (DLP), and inkjet printing (IJP) each impart distinct morphological signatures based on their unique deposition dynamics, material compatibility, and post-processing requirements. Deciphering these process–structure–property relationships is vital not only for electronic and sensing applications but also for emerging fields such as structured lubricants (Figure 7), where 3D-printed architectures are valued for their tailored surface properties, such as high lubricity and reduced wear rates.

From a manufacturing perspective, the advantages of 3D printing extend beyond electrochemical applications. This technology enables the integration of multiple materials within a single construct, independent of their chemical compatibility, thereby facilitating the development of complex hybrid designs.

Layer-by-layer deposition guided by CAD allows for precise control over structure, integration of dissimilar materials without chemical compatibility requirements, and simplified curing or sintering pathways [161–163]. These features make AM highly attractive for rapid prototyping, cost reduction, and scalable customization, with demonstrated competitiveness against traditional manufacturing in terms of resolution, speed, and mechanical integrity [164, 165].

Current 3D printing strategies can be broadly categorized into four major approaches: (a) inkjet printing, which dispenses materials with controlled pulses; (b) extrusion-based printing, which relies on mechanical deposition; (c) light-based printing, which uses lasers or light-emitting diodes (LEDs) [166]; and (d) stereolithography (SLA), in which a focused energy beam selectively heats a particular region in a liquid polymer bath to produce curing/printing. The different 3D printing processes are shown in Figure 8.

4.1 | Inkjet-Based 3D Printing

Inkjet-based 3D printing (IJP), also referred to as material or polymer jetting, has emerged as a versatile additive manufacturing technique for fabricating multi-material parts. Unlike conventional inkjet printing, which is restricted to single-layer deposition, IJP enables vertical structuring through a layer-by-layer approach, resulting in high precision and reproducibility of the final product [168]. This process relies on the deposition of liquid materials or solid suspensions under low-temperature and low-pressure conditions, guided by CAD-generated layouts processed using slicer software. This enables the fabrication of quasi-3D device architectures using a broad range of functional inks, including polymers, nanomaterials and composites [152].

Several jetting techniques, including piezoelectric, binder, electrostatic, hot-melt, and pneumatic jetting, offer comparable capabilities for achieving intricate designs with fine resolution [169]. To ensure structural integrity, a curing cycle follows each deposition step, with curing strategies tailored to ink chemistry. Low-temperature sintering with infrared lamps or photoinduced curing using visible or ultraviolet light have proven particularly effective, as they can be readily integrated into the printer setup and provide efficient solidification routes [170, 171]. Despite these advantages, IJP still faces several challenges. The droplet formation and dispensing process can be complex and unpredictable, often compromising process reliability and final product quality. Furthermore, the lack of robust droplet monitoring and process control tools continues to hinder reproducibility, despite ongoing efforts to improve their accuracy and adaptability [172].

Beyond single-material fabrication, IJP is increasingly leveraged for multi-material printing, enabling the integration of conductive, structural, and functional components into a single architecture. For instance, direct-ink-writing (DIW) combined with freeze casting has been used to produce MXene-based pressure sensors with hierarchical two-layer conductive networks that also serve as mechanical scaffolds, achieving >10 000 stable cycles while decoupling sensitivity from durability [173].
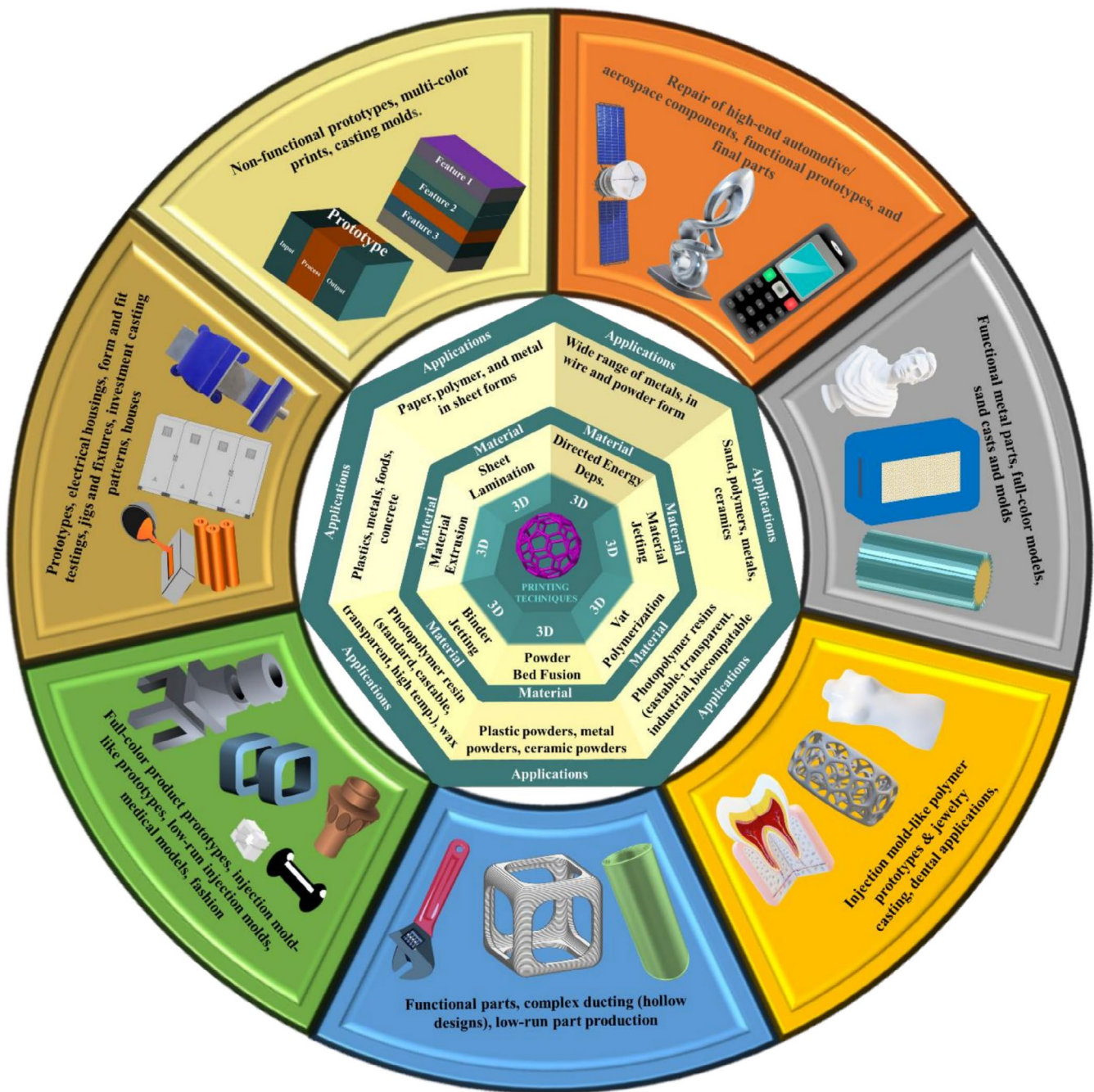
FIGURE 7 | Types and applications of 3D printing techniques.

Similarly, screen-printed PEDOT:PSS/MXene interdigitated electrodes integrated onto e-textile scaffolds demonstrated NFC-enabled readout and mechanical resilience across 21 400 bending cycles [174]. Other examples include stencil-printed graphene/TPU gauges embedded in PDMS matrices for motion monitoring over 5000 cycles [175] and layered MXene/PVDF-TrFE dielectric scaffolds combined with PEDOT:PSS/PDMS electrodes to create multi-material stacks with reliable 10 000-cycle performance [176]. Notably, inkjet-printed $Ti_3C_2T_x$ electrodes coated with ion-selective polymer membranes highlight the potential of IJP for wearable on-skin potentiometric sensing applications [177].

4.2 | Extrusion-Based Printing

Extrusion-based 3D printing has gained significant popularity for fabricating functional devices, owing to its versatility, affordability, and user-centric design [178]. Unlike conventional microfabrication approaches, extrusion printing enables the direct fabrication of complex structures, including light-emitting devices, without requiring sterile environments or cleanroom facilities [179]. Its versatility stems from the use of a wide range of printable materials that can be processed under relatively simple conditions. In extrusion-based printing, a polymer or ink is dispensed through a nozzle under pneumatic pressure, mechanical
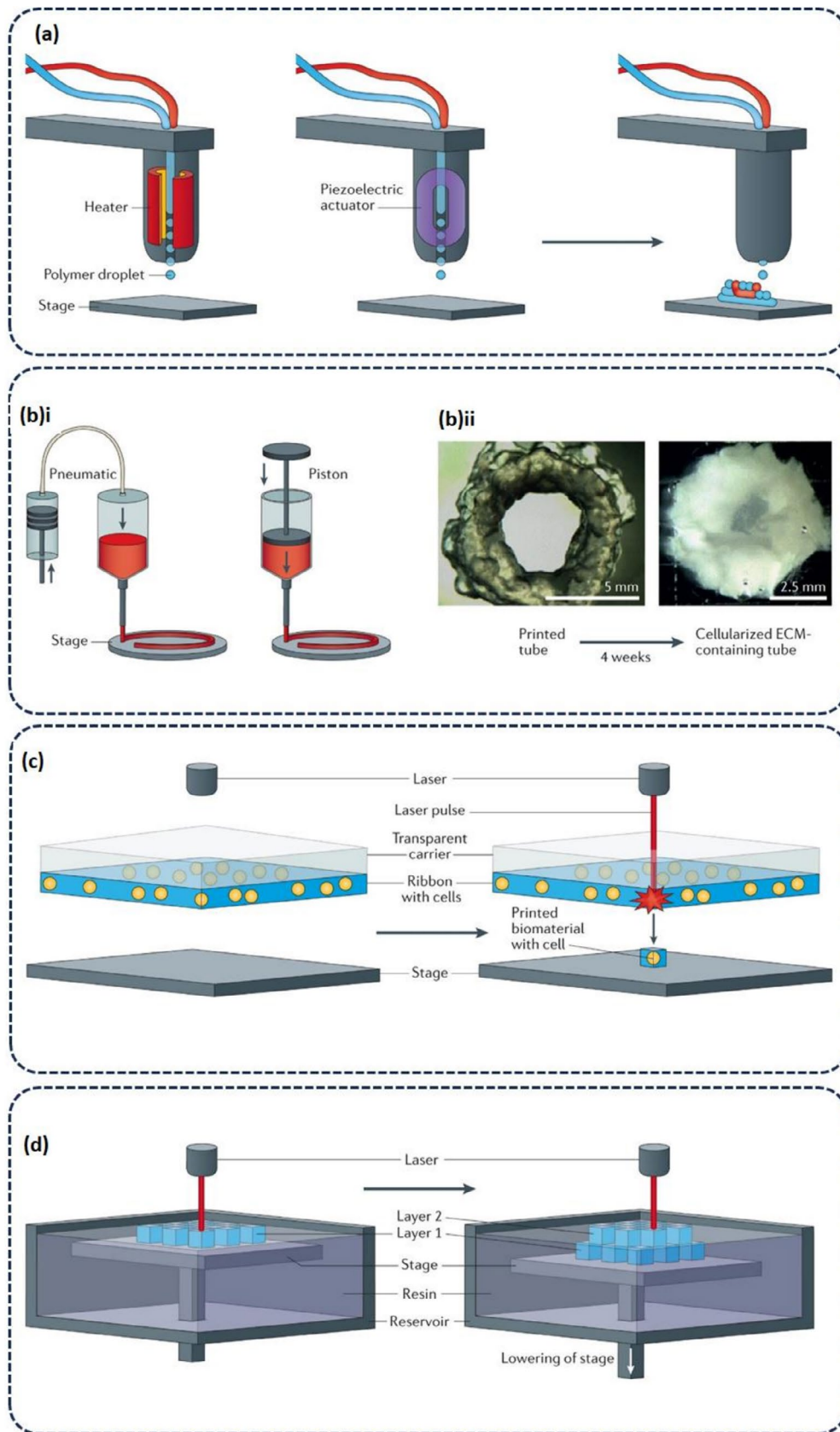
FIGURE 8 | 3D printing techniques (a) inkjet printing, (b) extrusion-based printing, (c) light-based printing, and (d) stereolithography [167].

pistons, or screw-driven systems. The material is continuously extruded in a controlled manner and deposited layer-by-layer to form 3D structures [180–182].

Compared with inkjet printing, this method accommodates higher-viscosity inks and semi-solid materials, significantly expanding the range of functional feedstocks. Depending on the system, the precursor material can be supplied as a liquid ink or as a thermoplastic filament that is melted prior to deposition, as in fused filament fabrication [181]. Among extrusion-based methods, FDM and DIW are the two techniques particularly relevant to biomedical applications. FDM employs thermoplastic filaments that are heated and extruded to create layered structures, whereas DIW uses specialized inks with tunable rheological properties to achieve precise deposition [183]. Both methods have demonstrated considerable potential for fabricating biomedical microdevices, offering high resolution and adaptability to various functional materials. DIW and FDM differ primarily in their material delivery mechanisms, with DIW requiring rheologically engineered inks and FDM relying on thermoplastic filaments [184].

4.3 | Light-Based 3D Printing

Light-assisted 3D printing techniques, such as SLA and DLP, have emerged as powerful alternatives to extrusion- and inkjet-based printing due to their speed, precision, and reliability. Unlike extrusion or inkjet methods, laser sintering and other light-driven approaches do not rely on print heads, thereby avoiding common issues such as nozzle clogging and enabling more consistent fabrication of complex architectures [167].

SLA was one of the earliest light-based 3D printing methods, relying on photopolymerization to solidify liquid resins into solid structures. In this process, a laser selectively cures resin layer by layer within a tank, gradually building the final 3D object [183, 185]. Photocuring, the fundamental mechanism underlying SLA, converts liquid resins into crosslinked solid networks under controlled light exposure. This process is widely regarded as the most accurate and precise additive manufacturing approach for fabricating intricate geometries [186]. Over time, SLA has evolved into several subcategories, among which DLP has gained significant attention owing to its improved speed and versatility [187].

DLP employs a digital micromirror device (DMD) or projector to simultaneously cure the entire resin layers rather than tracing individual points with a laser, as in SLA. The workflow typically involves slicing a 3D model into thin layers, projecting each layer pattern onto a photocurable resin bath, and incrementally raising the build platform to enable sequential curing [188]. This layer-wide curing accelerates printing dramatically while maintaining high resolution. Importantly, recent research has expanded the scope of DLP by enabling multi-material fabrication, allowing the production of objects with tunable mechanical strength, conductivity, flexibility, and bioactivity [189]. Although SLA and DLP share the same fundamental principle of light-induced crosslinking of liquid resins, their technical differences lie in the mode of light delivery and curing efficiency. SLA relies on a laser spot that scans across the resin, progressively

building lines and surfaces, whereas DLP cures an entire 2D image at once, making it significantly faster [190].

DLP and SLA are two widely used 3D printing technologies that fabricate objects through the photopolymerization of liquid resins. Their primary distinction lies in the light source and corresponding curing mechanism. SLA employs an ultraviolet laser that cures the resin in a point-by-point, rastering pattern to construct each layer. In contrast, DLP uses a digital projector screen to flash a single, complete image of each layer into the resin vat, curing the entire plane simultaneously. This fundamental difference in photopolymerization strategy makes DLP generally faster than SLA for most builds. The selection between these two methods is therefore contingent on the specific requirements of a project, such as the need for speed (DLP) versus potentially higher feature resolution (SLA) [191]. Figure 9 illustrates the stepwise workflow for fabricating 3D-printed electrochemical sensors and cells.

A critical advancement in 3D-printed electrochemical devices is the rheological behavior of inks, which governs printability, structural fidelity, and electrochemical performance. Shear-thinning fluids exhibit a decrease in apparent viscosity (η) with increasing shear rate ($\dot{\gamma}$), whereas thixotropic inks recover their viscosity over time after the stress is removed. For printable hydrogels, a power-law index < 1 and $\geq 90\%$ storage modulus recovery in three-interval thixotropy tests are typical benchmarks [193]. During extrusion, inks must flow under shear to prevent nozzle clogging and rapidly solidify to preserve voxel shapes and design resolution. For instance, graphene oxide (GO)/chitosan inks display a two-order-of-magnitude viscosity reduction at $\dot{\gamma} \approx 10^2\,s^{-1}$ but recover ~94% of their elastic modulus within seconds, producing crack-free filaments and uninterrupted electron pathways [194]. Nitrogen-doped carbon nanofibre/MWCNT gels exhibit similar rapid recovery, maintaining vertical layer integrity and preventing delamination [195]. Rheology also dictates the dispersion of active materials and electrochemical site density. In alginate/gelatin systems, increasing GO content improves shear-thinning but may induce agglomeration, leading to spatially uneven current distribution [196]. In contrast, additive-free graphene pastes tuned to $1–10^3\,Pa\cdot s$ at $\dot{\gamma} = 0.1\,s^{-1}$ printed continuous aerogel lattices with uniform conductive coatings, achieving areal capacitances of ~100 mF·cm^{-2} [197, 198].

Poorly matched rheology has the opposite effect on the results. Over-viscous inks ($\eta > 10^3\,Pa\cdot s$ at low shear) fracture, leaving micro-cracks that increase charge-transfer resistance, while under-viscous (nearly Newtonian) formulations slump after deposition, creating thickness gradients that widen the spread of k^0 and inflate double-layer noise. Studies on printed $Ti_3C_2T_x$/cellulose lattices show that only the rheology-optimized ink ($n \approx 0.3$, yield stress $\approx 400\,Pa$) delivers high-fidelity struts that translate into a two-fold gain in areal capacitance relative to poorly optimized counterparts [199]. Recent electrochemical examples reinforce the link between rheology and sensing metrics. RGO micro-electrodes with 35-μm smooth walls produced by direct-write GO inks that recover their viscosity in 0.5 s after extrusion show k^0 values one order of magnitude higher than drop-cast controls, while nitrogen-rich thick-carbon inks that combine shear thinning with fast thixotropy sustain a 70% higher signal-to-noise ratio over 5000 cycles [198, 199].
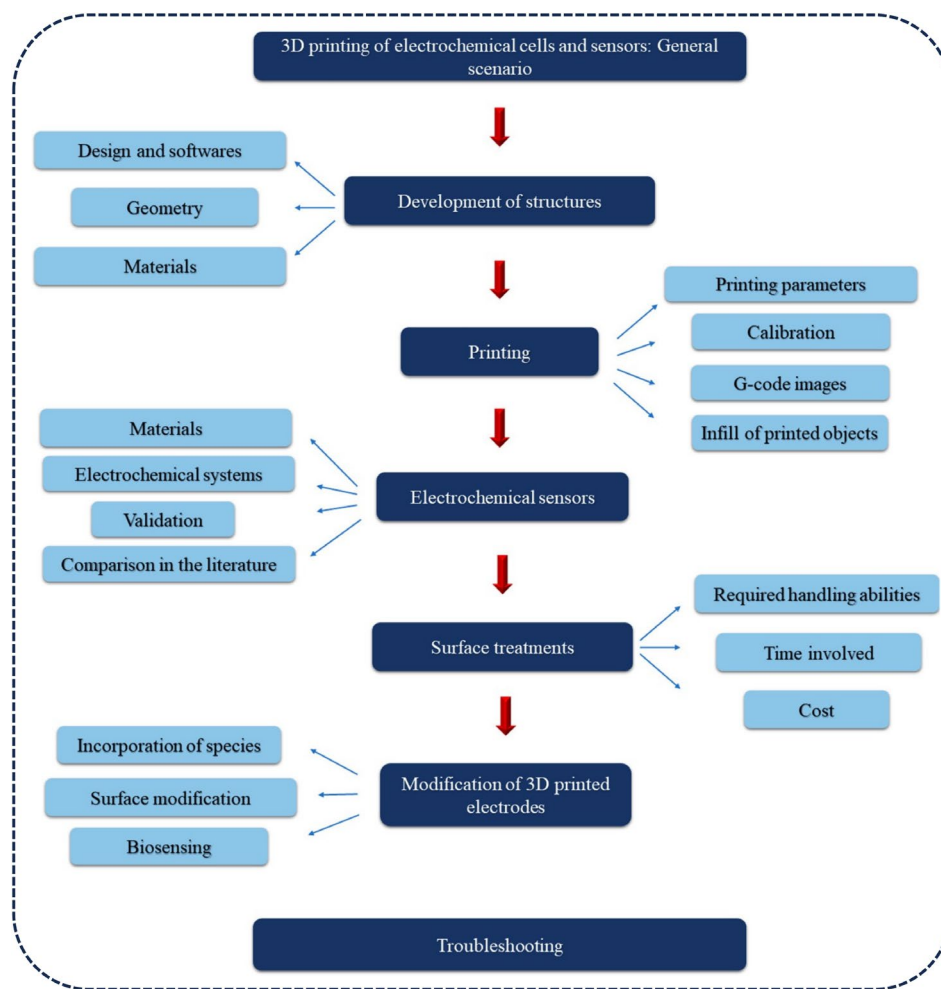
FIGURE 9 | Scheme of the main steps for developing 3D printed electrochemical sensors or cells [192].

Therefore, precisely aligning the shear-thinning and thixotropic profiles of the ink with the print path is a prerequisite for creating sensing layers with uniform morphology, absence of cracks, and high density of electroactive sites. These conditions are essential for enhancing the electron transfer kinetics and minimizing the baseline noise in practical biosensors. Rheological tuning is essential before selecting the most suitable 3D printing method (extrusion-based, inkjet, or photopolymerization) to achieve optimal structural and electrochemical performance. Table 3 summarizes these methods, detailing their resolution limits, material compatibility, cost-effectiveness, biosensor fabrication potential, and limitations. The intrinsic characteristics of each technique ultimately define the achievable feature size, material integration, and overall device performance.

In addition to their performance, additive manufacturing offers notable economic advantages over conventional microfabrication. Inkjet, direct-ink writing, screen printing, and desktop 3D printing circumvent the need for masks and costly cleanrooms, enabling rapid design iterations without the need for multimillion-dollar photolithography facilities. Research-grade microfluidic DLP printers range from 15 to 30k USD, while accessible LCD photopolymerization systems cost as little as 150–600 USD [208]. Contact printing allows higher throughput but requires an initial investment in physical masters, whereas non-contact approaches facilitate rapid pattern modification for small-batch manufacturing without master fabrication [209].

5 | Selecting Potential 2D Materials for 3D Printing

The strategic selection and formulation of 2D materials for use in 3D printing have emerged as pivotal factors enabling the creation of next-generation devices for information processing and sensing applications. Although advances in 3D printing have broadened accessibility and reduced costs, contemporary printers are often restricted to producing predominantly planar constructs with limited resolution, thereby constraining their utility. The development of 3D printing equipment has made it easier and cheaper to use, leading to rapid growth in its applications across various fields. To meet printing standards, the inks used must have correct consistency and flow properties. This requires high viscosity and specific rheological properties. Selecting appropriate materials to set the printing ink is crucial for successful printing [210]. Thus, the careful selection of materials for ink preparation has gained significant attention, particularly in sensing applications, where their unique electronic, mechanical, and surface properties hold considerable promise. Recent progress in

TABLE 3 | Comparative analysis of four 3D printing methods (inkjet drop-on-demand, extrusion-based, stereolithography (SLA/DLP), and two-photon polymerization (2PP/DLW)) is presented for electrochemical biosensor fabrication.

Method	Typical printing resolution	Compatible materials/ viscosity window	Relative cost-effectiveness (qualitative)	Biosensor suitability (examples)	Key limitations
Inkjet (drop-on-demand)	Picoliter droplets ($\approx$1–100 pL) enabling features in the tens of μm; practical lines $\gtrsim$30–100 μm depending on spreading [131, 200]	Low-viscosity functional/bio-inks ($\approx$2–50 mPa·s; bio-inks $\approx$3.5–12 mPa·s); requires small particles and filtration [131, 201, 202]	Moderate capital; non-contact, maskless deposition reduces process steps and reagent waste [203]	Gentle, non-contact patterning of enzymes/ antibodies/aptamers; localized deposition on electrodes/microchannels; fully printed enzyme sensors demonstrated [203]	Limited to low-viscosity inks; coffee-ring effects; nozzle drying/clogging; thick layers require multiple passes [131]
Extrusion-based (DIW/ robocasting/FDM)	Device-scale features typically > 50 μm (nozzle-limited) [200]	Broad window; shear-thinning, yield-stress pastes/ gels; $\approx$10^{-1}–10^{4} Pa·s; high solids loading tolerated [204]	Low–medium tool cost; high material latitude and throughput for meso-scale features [204]	Thick, low-resistance conductive traces (nanocarbon/metal-filled), elastomeric/ hydrogel structures, integrated housings [204]	Resolution ceiling set by nozzle ID and filament swelling; particle jamming/ clogging; rheology must be tuned for shape fidelity [204]
SLA/DLP (vat photopolymerization)	XY $\approx$10 μm; valves as small as 15 μm; ultra-small channels via exposure-control [200]	Photocurable resins (acrylates, PEGDA, elastomeric) for transparent microfluidic bodies [200]	Low per-part cost; rapid prototyping; cost-effective for POCT microfluidics [200]	Transparent microchannels/ valves, alignment fixtures, smooth chip housings (Ra $\sim$0.35 μm) [200]	Limited conductive/responsive materials; resin choice and post-processing required for biocompatibility; residual resin removal critical [200]
Two-photon polymerization (2PP/DLW)	Sub-μm down to $\approx$25–82 nm lines in optimized resists [205]	Specialized photoresists (low filler tolerance); hydrogel variants $\approx$1 μm features [206]	Poor cost-effectiveness for large parts; slow serial writing; tiny build volumes	Nanoscale transducers (nanogaps, plasmonic/ photonic templates), high-precision probe geometries [205, 207]	Very slow throughput; small build fields; conductivity integration often requires post-metallization [200]

17 of 33

solution-processed electronics has further accelerated the integration of these materials into scalable and versatile printing platforms, enabling researchers to optimize ink formulations through careful selection of binders, solvents, and additives [211]. Ultimately, successful 3D printing relies on aligning the printing conditions, filament quality, and material selection with the performance requirements of the intended device or component. The incorporation of 2D materials into 3D printing has opened new opportunities for developing high-performance electrochemical sensors with enhanced adaptability and functionality.

In particular, 2D materials such as graphene, TMDs, and MXenes have been explored for integration into electrochemical devices [212]. These materials have attracted significant academic and industrial interest owing to their distinctive features, such as biocompatibility, tunable surface chemistry, rapid electron transfer kinetics, and high surface-to-volume ratios. Importantly, their processability in liquid-phase dispersions makes them particularly well suited for printing technologies. Printing-compatible dispersions allow the exploitation of both structural and non-structural deposition techniques, including spin coating, drop casting, and inkjet or aerosol-based methods, offering a versatile platform for device fabrication [213].

The formulation of inks represents a central challenge, as it dictates critical parameters such as flow characteristics, drying dynamics, adhesion to the substrate, and overall film quality. Optimizing solvent systems to match the surface energy of 2D crystals improves their dispersibility and reduces artifacts, such as coffee-ring effects, during drying. For instance, the combination of isopropanol with 2-butanol has been shown to promote uniform deposition through Marangoni flow control. Similarly, selecting environmentally benign solvent mixtures with tailored Hansen solubility parameters enhances the dispersion stability of graphite and TMDs, enabling reliable large-area printing [214, 215]. Surfactants, such as sodium cholate, SDS, SDBS, and nonionic Pluronics, as well as $\pi-\pi$ anchoring polymers like pyrene-functionalized binders, further stabilize dispersions by providing electrostatic or steric repulsion while minimizing unwanted residues after printing [216, 217]. Additional improvements can be achieved through controlled exfoliation, flake size fractionation, and careful tuning of lateral dimensions and thickness to ensure nozzle compatibility and film uniformity. For MXenes, specific challenges, such as oxidation susceptibility, require hydrophilic solvent systems combined with antioxidant additives and storage under cool, dark conditions to preserve flake integrity and ink performance [218].

The selection of 2D materials must match the rheology of the ink, as well as the particle size and thermal or chemical stability of the selected printing method used. DIW requires shear-thinning viscoelastic gels with a yield stress sufficient to retain structural fidelity after extrusion. MXene- and graphene-based inks at high solid contents can achieve viscosities on the order of 10^3 Pa·s, making them suitable candidates [218]. In contrast, inkjet printing requires low-viscosity (1–20 mPa·s) stable inks with submicron flakes to avoid nozzle clogging, while maintaining surface tensions in the range of 20–50 mN/m to ensure droplet stability [219]. Aerosol jet printing accommodates a broader viscosity range (1–1000 cP) and supports larger flakes and non-planar patterning, though inks still require tailored dispersants and solvents to preserve conductivity and interpass adhesion [220]. For SLA and DLP, UV-curable resins with viscosities between 200 and 1000 mPa·s are typically employed; however, the incorporation of 2D fillers, such as GO, must be carefully controlled to preserve light penetration and prevent aggregation [221]. In fused filament fabrication (FFF), the selection of thermally stable 2D fillers with particle sizes smaller than the nozzle diameter and shear-thinning characteristics is essential for achieving smooth extrusion and consistent mechanical properties [222]. Conductive 2D materials, such as graphene and $Ti_3C_2T_x$, are particularly attractive when coupled with ink chemistries that minimize insulating residues after deposition or post-processing, thereby ensuring high electrical conductivity [218].

A persistent challenge across all these approaches is ensuring the long-term stability of 2D-material-based inks and printed structures. Stability is often demonstrated at the material level; for example, free-standing $Ti_3C_2T_x$ MXene films stored for up to a decade showed reversible conductivity loss due to water adsorption, which was recoverable through drying, highlighting the role of packaging and controlled dehydration in extending operational lifetimes [223]. Similarly, DIW-fabricated MXene sensors exhibit high cycling endurance, though long-term drift during extended use, particularly in wearable or hydrogel-based environments, remains insufficiently studied. Protective strategies, such as integrating catechol-functionalized MXenes with anti-dehydration hydrogels, have shown promise in preserving conductivity, moisture retention, and self-healing capabilities, though operational stability beyond several months has not yet been established [173, 224–226]. Reports of partial durability have been demonstrated in several deployment-ready printed systems. For instance, inkjet-printed $Ti_3C_2T_x$ electrodes maintained ion-selective performance over 50 days but suffered from a ~19% resistance increase, whereas printed graphene strain sensors sustained thousands of cycles but lacked extended studies on drift under physiological conditions. Similarly, aerosol-printed MoS_2 humidity sensors have demonstrated short-term reliability but lack multi-week drift analysis [175, 177]. Therefore, a thorough evaluation of these stability trends and their interactions with printing parameters is essential for selecting the optimal combination of 2D material and ink chemistry for a given application and fabrication method.

Ultimately, the formulation of robust application-specific inks requires balancing solvents, binders, additives, and 2D materials to ensure compatibility with printing methods while preserving functionality. Such formulations support the fabrication of intricate 3D architectures, enabling scalable and cost-effective manufacturing of advanced miniaturized devices [113]. The integration of 2D materials into 3D printing platforms not only improves performance metrics but also expands the design space for electrochemical sensors, paving the way for versatile, high-performance sensing technologies with broad industrial and biomedical applications.

6 | Application of 2D Materials in 3D Printing for Electrochemical Detection

The rapid expansion of 3D-printed electronics has driven increasing demand for advanced 2D material inks, which are being developed for a wide range of industrial applications, including energy harvesting, sensing, flexible displays, and smart packaging [213]. Among these, electrochemical detection is particularly promising, as 3D printing enables the integration of complex architectures, whereas 2D materials provide tunable functionalities.

Although the rational design of ideal multifunctional materials remains an ongoing challenge, 2D materials (graphene and TMDs) offer unique opportunities to overcome the current limitations. Their intrinsic physicochemical properties, such as high electrical conductivity, large surface-to-volume ratios, and tunable defect chemistry, make them attractive candidates for next-generation electrochemical applications [227]. In particular, 3D printing technologies can exploit these features to construct heterostructures in which distinct 2D layers contribute to complementary electronic, optical, or mechanical properties. This strategy not only enhances the versatility of 2D materials but also provides a practical route for the fabrication of high-performance hybrid systems.

An especially promising direction is the development of smart materials for 3D printing, where materials are engineered to respond to external stimuli via controlled deformation. The intrinsic structural flexibility of 2D materials allows fine-tuning of their properties by controlling the layer number, tailoring synthesis methods, defect and morphology engineering, as well as moiré and strain engineering. Such tunability is particularly relevant for next-generation electrochemical sensors, where sensitivity and selectivity are directly linked to nanoscale material properties [228]. The fabrication of heterostructures from multiple 2D materials further enhances their application by combining distinct functionalities into a single hybrid system. These heterostructures often exhibit unique electronic, optical, and mechanical properties that surpass those of their individual constituents. They can be readily synthesized using techniques such as van der Waals assembly or chemical vapor deposition, enabling the systematic manipulation of 2D material properties and expanding their application space. This strategy provides an effective pathway to overcome the intrinsic limitations of single 2D materials, thereby accelerating the advancement of 2D material-based technologies [229].

6.1 | Graphene and Its Composites

Graphene has emerged as a highly promising material for the development of 3D-printed electrochemical sensors owing to its exceptional electrical conductivity, chemical stability, and rapid interfacial electron transfer properties [230]. These attributes make it particularly attractive for electrochemical sensing applications, where fast and sensitive responses are essential. Real-world evaluations have demonstrated that graphene-based sensors can achieve sub-second response times, with laser-induced graphene (LIG) glucose electrodes showing response

times below 0.5 s and heterogeneous electron transfer rate constants in the range of 0.025–0.034 cm s^{-1} [231, 232]. Similarly, fast-scan cyclic voltammetry performed at carbon nanomaterial microelectrodes enables millisecond-scale monitoring of analytes, highlighting the capacity of graphene to facilitate rapid electrochemical processes. Comparative studies further highlight that LIG and other binder-free porous graphene electrodes deliver superior charge-transfer kinetics and higher sensitivity compared with conventional binder-rich screen-printed electrodes [233]. In dopamine sensing, graphene-based electrodes have achieved nanomolar detection limits and broad linear ranges, primarily due to favorable adsorption and accelerated charge transfer, outperforming traditional thick-film electrodes [234].

The capabilities of AM for high-speed and high-sensitivity sensor production, combined with DIW techniques for printing graphene materials, pave the way for cost-effective fabrication of advanced electrochemical sensors. Despite its exceptional electrical conductivity and large surface area, the direct use of pristine graphene in printing processes remains challenging due to the strong van der Waals forces between atomic layers, which hinder stable dispersion in liquid media. To improve the printability of graphene slurries, polymeric binders are often employed, as they facilitate ink formulation and extrusion. However, this strategy introduces significant trade-offs, as the binders may block the electrochemically active surface, thereby compromising the electrical performance and sensing capabilities of printed structures [235]. To address these drawbacks, chemical modification of graphene to GO has emerged as a practical alternative. The introduction of oxygen-containing functional groups enhances hydrophilicity, enabling GO to disperse more readily in aqueous solutions, making it the preferred precursor in most DIW studies of graphene-based inks. Nonetheless, the insulating nature of GO limits its application in electrochemical devices. To restore conductivity, printed GO structures are typically reduced using thermal or chemical methods to produce rGO, resulting in architectures with significantly improved electrical performance [236–238]. Ali and colleagues developed a highly sensitive biosensor for COVID-19 antibody detection by integrating 3D nano-printing with rGO nanoflakes and viral antigens. The fabrication process involved printing 3D electrodes, subsequently coating them with rGO nanoflakes, and functionalizing the surfaces with specific SARS-CoV-2 antigens. The resulting device, housed within a standard electrochemical cell coupled to a microfluidic system, detects antibody–antigen interactions via impedance spectroscopy. Remarkably, the biosensor achieved detection limits as low as 2.8×10^{-15} M for the spike S1 protein and 16.9×10^{-15} M for the receptor-binding domain, with results accessible through a smartphone interface. Furthermore, the platform supports low-pH regeneration, enabling repeated use without loss of specificity. This combination of reusability, portability, and ultrahigh sensitivity highlights its potential not only for COVID-19 diagnostics but also for broader applications in detecting other infectious diseases, including Ebola, HIV, and Zika [239].

3D printing with graphene enables the production of electrochemical sensors with complex shapes and geometries, which is impossible using traditional manufacturing methods. This

opens new possibilities for the design and optimization of electrochemical sensors, leading to improved performance and functionality. Recently, Sanati et al. developed a conductive ink based on chitosan and rGO, which enabled the fabrication of paper-based electrodes. Optimal performance and stability were achieved at a chitosan-to-GO ratio of 0.2. Using this formulation, they created a simple glucose sensor capable of detecting concentrations between 0.5 and 4 mM with high accuracy and precision. The device demonstrated strong stability and selectivity, remaining unaffected by interfering substances, thus demonstrating the potential of this ink for disposable sensors and flexible electronics [240]. In a complementary approach, Stefano et al. introduced a method for producing highly conductive filaments by combining graphite with PLA, followed by recrystallization, drying, and extrusion. These filaments, designed for 3D printing, enabled the direct fabrication of electrochemical sensors without additional surface treatment. The sensors reliably quantified uric acid (0.5–150.0 μmol L^{-1}) and dopamine (5.0–50.0 μmol L^{-1}) with detection limits as low as 0.07 μmol L^{-1} and 0.11 μmol L^{-1}, respectively. Furthermore, the platform was successfully extended to SARS-CoV-2 protein detection, achieving a linear range of 5.0–75.0 nmol L^{-1} and a detection limit of 1.36 nmol L^{-1}, with a sensitivity of 0.01 μA μg^{-1} mL. This new method for making conductive filaments has great potential for fabricating other 3D-printed conductive devices in the future [241].

The addition of oxygen-containing functional groups onto graphene sheets enhances sensor performance by optimizing the balance between functionalization and electrical conductivity, enabling effective interactions with target analytes [242]. Katic et al. developed 3D-printed graphene electrodes functionalized with Prussian blue (3DGrE/PB) through a multistep integration process, with structural and compositional characterization confirmed via SEM, AFM, and spectroscopic techniques. Compared to conventional electrodes (glassy carbon, gold, and platinum), the 3DGrE/PB system demonstrated superior electrocatalytic activity toward H_2O_2 reduction. In practical applications involving real samples (milk and mouthwash), the electrodes achieved an LOD of 0.11 μmol L^{-1}, a limit of quantification of 0.37 μmol L^{-1}, and an analytical frequency of 87 h^{-1}, thereby enabling rapid and precise quantification of peroxide. These results demonstrate a scalable approach for producing conductive electrodes for practical molecular sensing applications (Figure 10a) [243]. To address the challenge of poor conductivity in 3D-printed plastics, Estadulho et al. developed low-cost monolithic electrochemical sensors by electrochemically growing polyaniline on PLA embedded with graphite traces. This approach converts an insulating body into a conductive one-piece device without requiring conductive filaments. Further functionalization with Ru and Cu electrodeposition enabled the quantification of caffeine, H_2O_2, and glucose with LODs of 57.7, 2.3, and 49.3 μmol L^{-1}, respectively, offering a rapid, inexpensive route for practical electrochemical analysis (Figure 10b) [244].

For heavy metal detection in water, Walters et al. reported the development of 3D-printed graphene/PLA electrodes designed for the quantification of Hg, Pb, and Cd. The electrodes were fabricated by inserting a 600 μm-diameter graphene/PLA filament into an epoxy-filled pipette tip and subsequently characterized using electron microscopy, Raman spectroscopy, and cyclic voltammetry. Using anodic stripping voltammetry, Hg was detected at concentrations as low as 6.1 nM (1.2 ppb) in both 0.01 M HCl and 0.1 M acetate buffer, whereas Pb and Cd could not be quantified at concentrations below 400 nM. The sensitivity toward these metals was significantly enhanced through surface modification with bismuth microparticles, yielding clear stripping peaks at concentrations as low as 20 nM. This improvement lowered the detection limits to 4.1 ppb for Pb^{2+} and 2.2 ppb for Cd^{2+}, thereby enabling the quantification of all three metals at levels below the U.S. EPA action limits for drinking water (Figure 10c) [245].

Hassan et al. introduced a sustainable strategy for fabricating graphene inks optimized for 3D printing by incorporating polymer binders and non-toxic solvents to address the challenges associated with high ink viscosity. These inks enable the production of high-performance sensing devices for VOCs. Owing to a tenfold increase in the surface area-to-volume ratio achieved through 3D printing, the devices exhibited significantly improved resolution, sensitivity, and selectivity and were capable of detecting VOCs, such as ethanol, at concentrations as low as 5 ppm at 20°C (Figure 10d) [246]. These findings affirm the potential of graphene-based inks for the scalable production of electrochemical biosensors, demonstrating how 3D printing can advance graphene-enabled sensing technologies.

6.2 | TMDs and Their Composites

TMDs, with the general formula MX$_2$ (where M = Mo or W and X = S, Se, or Te), have attracted significant attention as graphene-like materials with superior mechanical, electrical, and optical properties. Unlike zero-bandgap graphene, TMDs exhibit tunable bandgaps, high electrical conductivity, and distinctive optical responses, making them suitable for various electronics, energy storage, sensing, and biomedical applications [247]. Single-layer TMDs, such as MoS$_2$ and WS$_2$, have gained particular interest because of their direct bandgaps and desirable electronic properties. These materials have been successfully synthesized and explored for applications in nanoelectronics, nanophotonics, and nanoscale sensing [248, 249]. The exceptional properties of TMDs, including high stability, biocompatibility, rapid heterogeneous electron transfer, and large specific surface area, make them especially suitable for sensing applications, which has been increasingly recognized in recent literature [212]. Common TMDs include MoS$_2$, WS$_2$, MoSe$_2$, WSe$_2$, MoTe$_2$, and WTe$_2$, with MoS$_2$ being the most extensively studied owing to its robustness and stability compared with other 2D semiconductors [250]. Figure 11a illustrates the structural heterogeneity of two-dimensional TMD layers, encompassing intrinsic defects (vacancies, antisites, grain boundaries), phase transitions (2H ↔ 1T/1T'), van der Waals gap engineering through interlayer spacing or restacking, and architected vertical or lateral heterostructures formed by stacking or stitching dissimilar TMDs. The figure also highlights Janus TMD layers, in which distinct chalcogens occupy the top and bottom planes, breaking out-of-plane symmetry and imparting unique properties [251].
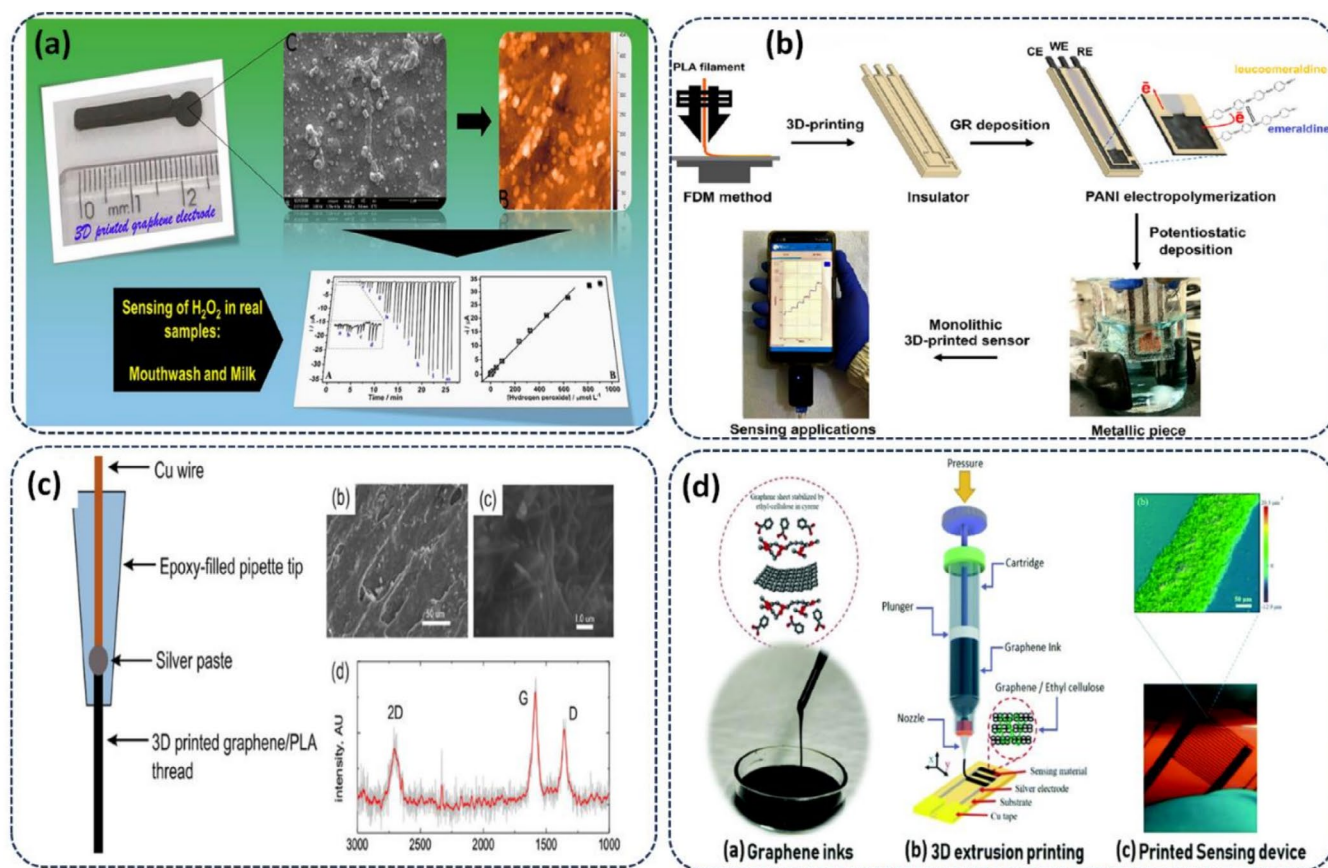
FIGURE 10 | (a) 3D-printed graphene electrodes modified with Prussian blue for peroxide detection [243] (b) illustrative scheme of production and application of monolithic 3D-printed sensor [244] (c) 3D-printed cylinder electrode for trace analysis of heavy metals [245] and (d) extrusion-printed sensors for VOCs [246].

Singh et al. built a 2D-MoS_2 microfluidic immunosensor by CTAB-assisted exfoliation to yield positively charged CTAB–MoS_2 nanosheets, enabling protein conjugation and electrostatic deposition on hydrolyzed ITO microelectrodes within a PDMS chip for *Salmonella typhimurium* detection via EIS. The device showed a sensitivity of 1.79 kΩ·CFU^{-1} mL cm^{-2}, a limit of detection of 1.56 CFU mL^{-1}, and a wide dynamic range of 10^1–10^7 CFU mL^{-1} [252] (Figure 11b). These results highlight the potential of MoS_2 nanosheets for developing highly sensitive microfluidic immunosensors for detecting foodborne pathogens. 2D TMD materials have unique catalytic and sensing properties, making them ideal for the fabrication of electrochemical LOC microfluidic devices. These devices are sought after for their potential applications in biodiagnostics and sensing. Toh et al. reported a simple drop-casting method to integrate four t-BuLi-exfoliated group 6 TMD materials (MoS_2, $MoSe_2$, WS_2, and WSe_2) into LOC devices. The performances of the materials for H_2O_2 detection were compared. The WS_2-based LOC device was the most effective of the four materials, displaying a wide range of linear responses (20 nM to 20 μM and 100 μM to 2 mM), a low detection limit (2.0 nM), and good selectivity for real sample analysis [255]. The outcomes of this study demonstrate the potential of electrochemical LOC microfluidics for application in the field of bio-diagnostics and sensing. With ease of integration, the use of electrochemical LOC microfluidics can be expanded in the future to enhance the development of new and innovative devices for various applications. The results of this

study are expected to provide new opportunities and insights into the development of 2D TMD-based electrochemical microfluidic devices.

MoS_2 nanocomposites are widely used as sensing substrates because of their unique characteristics. They can stabilize metal nanoparticles and generate local surface plasmon resonance, resulting in a strong plasma coupling effect and a high surface area for capturing antibodies. This makes them suitable for integration with microfluidic chips for use as biosensors. Qiu et al. engineered a self-assembled microfluidic immunoassay biochip using Lys-AuNPs@MoS_2 that generates digital solid-phase readouts with 2D target maps. It simultaneously quantifies six serum biomarkers (PCT, CRP, IL-6, cTnI, cTnT, and NT-BNP), processing 60 samples in 40 min with LOD in the few-to-tens of pg/mL range. The platform offers high throughput and sensitivity on a uniform surface, indicating its strong potential for clinical diagnosis (Figure 11c) [253]. Novčić et al. assessed thermally activated, 3D-printed nanocarbon/PLA electrodes after electrodepositing MoS_2, WS_2, and their heterojunctions for the hydrogen evolution reaction (HER) via linear sweep voltammetry. The MoS_2 coatings exhibited significantly higher catalytic activity than WS_2, and the heterojunction performance mirrored that of the outermost deposited layer. HER-active regions were near-surface to ~150 μm for MoS_2 and extended to ~300 μm for WS_2 (Figure 11d) [254]. These findings demonstrate that the
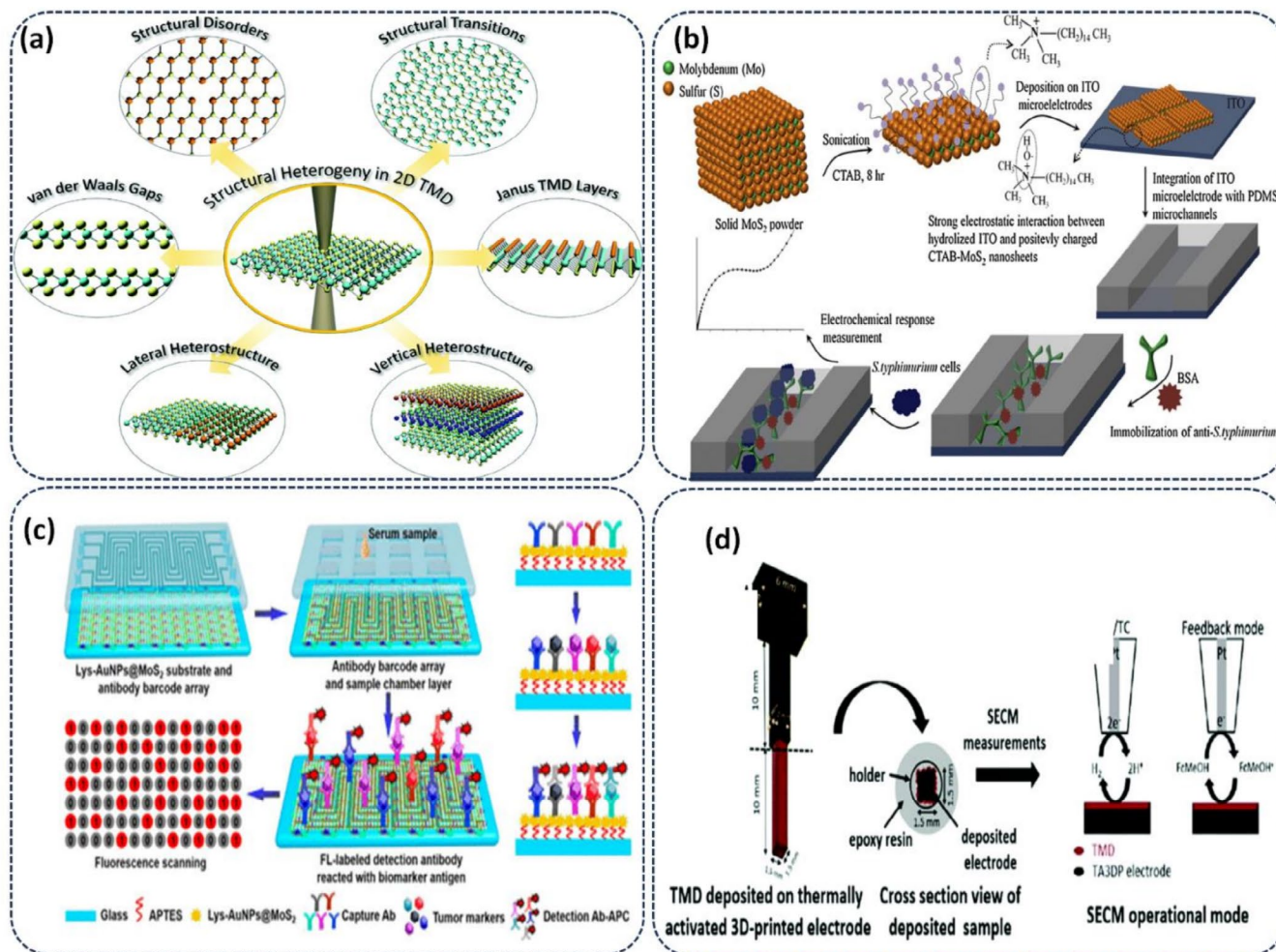
FIGURE 11 | (a) Schematic illustrations of the structural heterogeneity in 2D TMD layers [251]; (b) design of microfluidic biosensor for *S. typhimurium* detection [252]; (c) Lys-AuNPs@MoS$_2$ nanocomposite self-assembled microfluidic immunoassay biochip [253]; (d) cross-sectional sample preparation for SECM measurements [254].

electrodeposition and heterojunctions of different TMDs on 3D nanocarbon electrodes result in HER active sites located not only at the outer surface but also within the interior of the nanocarbon structure. This has the potential to significantly improve hydrogen production efficiency.

In addition, Wang et al. developed an ultrasensitive electrochemical Pb^{2+} sensor by coupling GR aptamer–functionalized 3D MoS$_2$ microspheres with AuPt-MCNT modified glassy carbon electrodes. Pb^{2+} induced aptamer cleavage enabled catalytic signaling, achieving a linear, selective response with a detection limit of 0.015 nM, demonstrating its potential for environmental and biological monitoring [256]. The continued development of TMD-based materials and composites holds significant potential for transforming the monitoring and control of chemical and biological processes.

6.3 | MXenes and Their Composites

MXenes are emerging as highly promising sensor materials because of their tunable bandgap properties and metal-like electrical conductivity. Structurally inspired by graphene and TMDs, MXenes consist of 2D carbides and nitrides of transition metals,

offering abundant active surface sites that enable high sensitivity and low detection limits in sensory applications. Their excellent electrical conductivity also reduces noise, further enhancing signal reliability, positioning MXenes as potential successors to conventional sensor technologies [257, 258]. MXenes possess hydrophilic surfaces and high metallic conductivity (~6000–8000 S cm^{-1}), allowing their application in various fields, such as energy storage, transparent electrodes, EMI shielding, sensors, and transistors. The major challenge hindering the application of MXenes is their poor ambient stability, which is due to oxidation in the presence of either water or oxygen [259]. 3D printing technologies have gained attention for assembling 2D materials, such as MXenes, into functional 3D aerogels owing to their simple fabrication, customized geometry and physical properties, and improved performance. The use of facile electrode fabrication methods aimed at hindering the restacking and aggregation of electrode materials is of great significance for improving electrode performance. For example, Tetik et al. combined unidirectional freeze casting and inkjet-based 3D printing to fabricate macroscopic porous aerogels with vertically aligned Ti$_3$C$_2$T$_x$ sheets. This method allows for easy control over the aerogel microstructure and alignment of MXene sheets, resulting in excellent electromechanical performance and the ability to withstand almost 50% compression before recovering to the original shape

while maintaining electrical conductivity. The addition of an inkjet-printed MXene current collector layer with horizontally aligned MXene sheets improved electrochemical performance. The cells showed the best results with a horizontal MXene current collector and subsequent vertical MXene sheet-alignment layer [260]. These advancements in print-guided alignment and porosity stabilization pave the way for integrating 3D-printed MXene electrodes with MXene quantum dots (MQDs) for highly sensitive dopamine sensing. For example, Wan et al. fabricated a 3DE from a graphene/PLA filament and functionalized it with MQDs to create a highly sensitive dopamine (DA) sensor. The 3DEs were characterized using scanning electron microscopy (SEM), X-ray photoelectron spectroscopy (XPS), and contact angle measurements, and their electrochemical behavior was evaluated using cyclic voltammetry (CV) and electrochemical impedance spectroscopy (EIS). The resulting sensor exhibited a DA detection range of 0.01–$20\,\mu$M with a 3 nM detection limit, along with high selectivity in practical sample analyses. This approach highlights the potential of integrating 2D material QDs into 3DE, opening new avenues for advanced biosensor design [261].

Beyond dopamine sensing, MXene-based heterostructures are also advancing biosensing technologies. MXene–MoS_2 2D–2D hybrids provide an ideal transducer platform by combining metallic $Ti_3C_2T_x$, which acts as a highly conductive "charge-transfer highway," with semiconducting MoS_2, which offers abundant adsorption sites and favorable band alignment. Ultrafast pump–probe spectroscopy revealed sub-150 fs charge/energy transfer from $Ti_3C_2T_x$ to MoS_2, along with long-lived excited carriers, consistent with the presence of a built-in interfacial electric field that lowers interfacial resistance and accelerates electron transfer [262]. For example, a miR-21 biosensor uses an MXene–MoS_2 scaffold to co-anchor AuNP-tethered hairpins and thionine. Through catalytic hairpin assembly (CHA), target binding generates abundant dsDNA near the interface, increasing the charge-transfer resistance and suppressing the thionine current in a signal-off configuration. This dual amplification (structural and biochemical) enables sensitive detection across the 100 fM–100 nM range, with an LOD of ~26 fM [86]. Similarly, electrochemiluminescence (ECL) sensors based on MoS_2-QD/MXene hybrids achieved LODs as low as 10 fM for exosomal miRNA-135b, demonstrating the broad applicability of conductive scaffolds and semiconducting emitter/adsorbent strategies for signal amplification [87].

Xiao et al. developed a highly sensitive electrochemical sensor for arsenic (III) by integrating MXene with amine-functionalized Fe-based metal–organic frameworks (Fe-MOFs), forming a Fe-MOF/MXene composite. The composite was synthesized in situ via a one-step hydrothermal process in the presence of MXene, which provided a large surface area and excellent electrical conductivity, thereby enhancing the electrochemical performance of the electrodes. When employed as a modifier, the Fe-MOF/MXene composite enabled the fabrication of an arsenite sensor with remarkable sensitivity. X-ray photoelectron spectroscopy confirmed the strong interaction between arsenic species and hydroxyl groups at the Fe-MOF/MXene interface, which contributed to the pronounced electrochemical response. Using square wave anodic stripping voltammetry, the Fe-MOF/MXene-modified electrode exhibited a significantly high current response to As(III), achieving both high sensitivity ($8.94\,\mu$A$\,($ng L$^{-1})^{-1}$cm^{-2}) and a low detection limit (0.58 ng L^{-1}). Moreover, the sensor demonstrated reliable performance in real water samples, highlighting its practical applicability in real-world applications. This study presents the synergistic advantages of combining MXenes with Fe-MOFs, offering a promising pathway for designing next-generation electrochemical sensors with superior sensitivity and detection capabilities [263].

In another study, Sharifuzzaman et al. developed a smart wound dressing incorporating multifunctional sensors for managing chronic wounds. The design involved the functionalization of 3D LGG sheets with 2D MXene nanosheets through covalent C—O—Ti crosslinking, yielding an LGG–MXene hybrid scaffold with enhanced conductivity and electrochemical performance. This scaffold was then integrated into a PDMS substrate to create a flexible and stretchable dressing capable of simultaneously monitoring uric acid (UA), pH, and temperature at the wound site. The UA sensor demonstrated rapid responsiveness with a sensitivity of $422.5\,\mu$A mM^{-1}cm^{-2} and a detection limit of $50\,\mu$M. The pH sensor exhibited a linear Nernstian response with a sensitivity of -57.03 mV pH^{-1}, while the temperature sensor showed a highly linear resistivity response (sensitivity: 0.09% °C^{-1}, $R^2 = 0.999$). In addition to its high sensing performance, the mechanical flexibility of the dressing allows it to conform to varying body movements and wound geometries, making it particularly suitable for patients with chronic wounds. By integrating multifunctional sensors, this platform enables real-time wound monitoring, which has strong potential to improve diagnostic precision, accelerate healing, and ultimately enhance therapeutic outcomes [264].

7 | Current Challenges and Future Outcomes

The rapid progress in science and technology has fuelled the growing demand for advanced, efficient, and miniaturized electronic products. Devices such as smartphones, health trackers, microsensors, and intelligent robots exemplify this shift toward smarter, more flexible, and compact electronic devices. The continual drive for miniaturization not only enhances device functionality but also contributes to improved standards of living and convenience of use. Looking ahead, further innovations in this field promise to deliver increasingly sophisticated and impactful technologies.

Among the emerging fabrication methods, 3D printing holds significant promise for advancing electrochemical device manufacturing. Its ability to create customized structures offers tremendous potential for improving the performance and functionality of devices. However, translating laboratory-scale research into practical applications remains challenging. Critical barriers include the optimization of ink formulations, curing strategies, ink distribution, and electrode geometries. Addressing these issues will require the design of conductive inks with precisely controlled compositions and viscosities, along with compatible substrates and post-processing treatments such as sintering, heating, and curing to ensure high conductivity and robust electroanalytical performance [27].

3D printing has already shown considerable promise in the fabrication of electrochemical and physical sensors. However, before widespread adoption, fundamental limitations such as low production efficiency, processing complexity, and restricted sensitivity/selectivity must be resolved. Developing advanced 3D electrode designs, incorporating novel materials, and refining sensor geometries are key to improving analytical parameters. The versatility of 3D printing also supports the use of diverse substrate types, from rigid ceramics and silica to flexible plastics and paper, thereby broadening potential applications. Moreover, the relatively low scalability of 3DE restricts its integration into high-performance biosensors [265].

Material design also plays a pivotal role in overcoming these bottlenecks. For instance, while the use of binders in 3D-printed architectures improves mechanical integrity, it often reduces the active surface area and adversely affects the electrochemical behavior. To address this, Xu et al. [266] demonstrated a 3D-printed silica sacrificial template that yielded bicontinuous porous graphene foams with exceptional surface area, electrical conductivity, and mechanical strength, which are essential for next-generation electrochemical devices. Moving toward large-scale implementation will require not only material innovation but also strategies that guarantee dimensional stability and sufficient mechanical robustness during mass production.

A key challenge lies in scaling up fabrication processes while maintaining device fidelity. Industrial-scale manufacturing demands integrated R2R architectures capable of producing multi-material stacks with high throughput and reproducibility. Successful implementation requires precise control over moving-web mechanics, tension zones, stack orthogonality, and registration accuracy, supported by high-contrast fiducials and metamodel-based optimization [93, 267]. Advances in low-temperature curing routes (UV, photonic, plasma) and solvent/thermal ladders, coupled with adhesion pretreatments and barrier interlayers, have already demonstrated stable conductor printing at speeds approaching 10 m/min, establishing a pathway for scalable sensor production [93, 267–269]. Furthermore, hybrid manufacturing strategies that combine high-throughput contact printing (gravure, rotary screen) for conductors/dielectrics with non-contact techniques (slot-die, inkjet) for membranes and late-stage biofunctionalization have been validated in pilot R2R systems [90, 270, 271]. Addressing electrochemistry-specific vulnerabilities, such as Ag/AgCl drift, electrolyte leakage, and instability in permselective films, will also be crucial, requiring careful ink/overcoat design, dielectric robustness, and dryer profile optimization [90, 91, 270, 271]. Inline quality control frameworks that integrate defect inspection, optical thickness measurements, electrical continuity testing, and real-time electrochemical surrogates are essential for stabilizing manufacturing variables and ensuring reproducibility at scale [92, 269].

Furthermore, the customization capabilities of 3D printing, particularly for 2D materials and hybrid composites, will unlock opportunities for fabricating multifunctional devices with unprecedented performance and versatility. As material design, ink formulation, and scalable processing strategies converge, 3D-printed electrochemical devices are ready to transition from proof-of-concept structures to robust, mass-manufactured products. Continued research and industrial integration will position 3D printing as a transformative platform for next-generation electronic and energy devices.

8 | Conclusion

The convergence of 2D nanomaterials with additive manufacturing is redefining the conception and fabrication of electrochemical sensors. By leveraging the unique physicochemical properties of graphene, TMDs, MXenes, and related materials, 3D printing enables bespoke electrode architectures, enhanced electron transfer kinetics, and multifunctional device integration, which were previously unattainable using conventional approaches. However, the path toward translation is contingent on addressing persistent hurdles in terms of ink formulation, long-term stability, and manufacturing scalability. Emerging strategies, such as rheology-tailored inks, hierarchical structuring, and hybrid contact/non-contact printing within roll-to-roll architectures, highlight promising routes to bridge laboratory demonstrations with real-world applications. Looking forward, interdisciplinary advances in materials chemistry, process engineering, and sustainable manufacturing are required to fully realize robust, high-throughput, and multifunctional electrochemical sensing platforms. The integration of 2D materials and 3D printing thus offers not only significant improvements but also a structural shift in the design paradigm of next-generation diagnostics, environmental monitoring, and smart electronics.

Author Contributions

Arshid Numan: conceptualization, writing – original draft. **Lijie Li:** visualization, supervision. **Salem AlFaify:** writing – review and editing, funding acquisition. **Muhammad Sheraz Ahmad:** writing – original draft, visualization. **Syam Krishnan:** writing – review and editing. **Mohammad Khalid:** writing – review and editing, funding acquisition.

Conflicts of Interest

The authors declare no conflicts of interest.

Data Availability Statement

No data were used in the research described in this study.

References

1. M. N. Islam and R. B. Channon, *Bioengineering Innovative Solutions for Cancer*, vol. 74 (Academic Press, 2019), 47, https://doi.org/10.1016/B978-0-12-813886-1.00004-8.

2. J. Baranwal, B. Barse, G. Gatto, G. Broncova, and A. Kumar, "Electrochemical Sensors and Their Applications: A Review," *Chem* 10 (2022): 363, https://doi.org/10.3390/chemosensors10090363.

3. N. J. Ronkainen, H. B. Halsall, and W. R. Heineman, "Electrochemical Biosensors," *Chemical Society Reviews* 39 (2010): 1747.

4. S. Singh, A. Numan, and S. Cinti, "Point-Of-Care for Evaluating Antimicrobial Resistance Through the Adoption of Functional Materials," *Analytical Chemistry* 94 (2021): 26–40, https://doi.org/10.1021/acs.analchem.1c03856.

5. A. Numan, S. Singh, Y. Zhan, et al., "Advanced Nanoengineered—Customized Point-Of-Care Tools for Prostate-Specific Antigen," *Microchimica Acta* 189 (2022): 27, https://doi.org/10.1007/s00604-021-05127-y.

6. Y. Z. Zhang, Y. Wang, T. Cheng, et al., "Printed Supercapacitors: Materials, Printing and Applications," *Chemical Society Reviews* 48 (2019): 3229–3264, https://doi.org/10.1039/c7cs00819h.

7. Y. Zhao, B. Wang, H. Hojaiji, et al., "A Wearable Freestanding Electrochemical Sensing System," *Science Advances* 6 (2020): 6, https://doi.org/10.1126/sciadv.aaz0007.

8. X. Zhang, *Flexible and Stretchable Triboelectric Nanogenerator Devices: Toward Self-Powered Systems* (John Wiley & Sons, 2019).

9. S. Choi, "Powering Point-Of-Care Diagnostic Devices," *Biotechnology Advances* 34 (2016): 321–330, https://doi.org/10.1016/j.biotechadv.2015.11.004.

10. S. Nayak, N. R. Blumenfeld, T. Laksanasopin, and S. K. Sia, "Point-Of-Care Diagnostics: Recent Developments in a Connected Age," *Analytical Chemistry* 89 (2017): 102–123, https://doi.org/10.1021/acs.analchem.6b04630.

11. S. Wang, M. A. Lifson, F. Inci, L. G. Liang, Y. F. Sheng, and U. Demirci, "Advances in Addressing Technical Challenges of Point-Of-Care Diagnostics in Resource-Limited Settings," *Expert Review of Molecular Diagnostics* 16 (2016): 449–459, https://doi.org/10.1586/14737159.2016.1142877.

12. J. Adkins, K. Boehle, and C. Henry, "Electrochemical Paper-Based Microfluidic Devices," *Electrophoresis* 36 (2015): 1811–1824, https://doi.org/10.1002/elps.201500084.

13. D. W. Kimmel, G. LeBlanc, M. E. Meschievitz, and D. E. Cliffel, "Electrochemical Sensors and Biosensors," *Analytical Chemistry* 84 (2012): 685–707.

14. M. Struzik, I. Garbayo, R. Pfenninger, and J. L. M. Rupp, "A Simple and Fast Electrochemical CO2 Sensor Based on Li7La3Zr2O12 for Environmental Monitoring," *Advanced Materials* 30 (2018): 1804098, https://doi.org/10.1002/adma.201804098.

15. F. Röck, N. Barsan, and U. Weimar, "Electronic Nose: Current Status and Future Trends," *Chemical Reviews* 108 (2008): 705–725, https://doi.org/10.1021/cr068121q.

16. S. Singh, N. Arshid, and S. Cinti, "Electrochemical Nano Biosensors for the Detection of Extracellular Vesicles Exosomes: From the Benchtop to Everywhere?," *Biosensors and Bioelectronics* 216 (2022): 114635, https://doi.org/10.1016/j.bios.2022.114635.

17. A. Hierlemann and R. Gutierrez-Osuna, "Higher-Order Chemical Sensing," *Chemical Reviews* 108 (2008): 563–613, https://doi.org/10.1021/cr068116m.

18. L. E. Kreno, K. Leong, O. K. Farha, M. Allendorf, R. P. Van Duyne, and J. T. Hupp, "Metal–Organic Framework Materials as Chemical Sensors," *Chemical Reviews* 112 (2012): 1105–1125, https://doi.org/10.1021/cr200324t.

19. T. Yang, D. Xie, Z. Li, and H. Zhu, "Recent Advances in Wearable Tactile Sensors: Materials, Sensing Mechanisms, and Device Performance," *Materials Science and Engineering R: Reports* 115 (2017): 1–37, https://doi.org/10.1016/j.mser.2017.02.001.

20. S. Naficy, F. Oveissi, B. Patrick, A. Schindeler, and F. Dehghani, "Printed, Flexible pH Sensor Hydrogels for Wet Environments," *Advanced Materials Technologies* 3 (2018): 1800137, https://doi.org/10.1002/admt.201800137.

21. P. H. Lin and B. R. Li, "Antifouling Strategies in Advanced Electrochemical Sensors and Biosensors," *Analyst* 145 (2020): 1110–1120, https://doi.org/10.1039/c9an02017a.

22. C. Carrell, A. Kava, M. Nguyen, et al., "Beyond the Lateral Flow Assay: A Review of Paper-Based Microfluidics," *Microelectronic Engineering* 206 (2019): 45–54, https://doi.org/10.1016/j.mee.2018.12.002.

23. L. Wang, X. Fu, J. He, et al., "Application Challenges in Fiber and Textile Electronics," *Advanced Materials* 32 (2020): 1901971, https://doi.org/10.1002/adma.201901971.

24. H. N. Chan, M. J. A. Tan, and H. Wu, "Point-Of-Care Testing: Applications of 3D Printing," *Lab on a Chip* 17 (2017): 2713–2739, https://doi.org/10.1039/c7lc00397h.

25. B. Li, S. Zhang, L. Zhang, Y. Gao, and F. Xuan, "Strain Sensing Behavior of FDM 3D Printed Carbon Black Filled TPU With Periodic Configurations and Flexible Substrates," *Journal of Manufacturing Processes* 74 (2022): 283–295, https://doi.org/10.1016/j.jmapro.2021.12.020.

26. A. Dijkshoorn, P. Werkman, M. Welleweerd, et al., "Embedded Sensing: Integrating Sensors in 3-D Printed Structures," *Journal of Sensors and Sensor Systems* 7 (2018): 169–181, https://doi.org/10.5194/jsss-7-169-2018.

27. V. Katseli, A. Economou, and C. Kokkinos, "Single-Step Fabrication of an Integrated 3D-Printed Device for Electrochemical Sensing Applications," *Electrochemistry Communications* 103 (2019): 100–103, https://doi.org/10.1016/j.elecom.2019.05.008.

28. R. Amin, S. Knowlton, A. Hart, et al., "3D-Printed Microfluidic Devices," *Biofabrication* 8 (2016): 022001, https://doi.org/10.1088/1758-5090/8/2/022001.

29. K. Agashe, A. Sachdeva, and S. Chavan, "3D Printing and Advance Material Technology," *International Journal of Grid and Distributed Computing* 13 (2020): 1899.

30. T. Han, S. Kundu, A. Nag, and Y. Xu, "3D Printed Sensors for Biomedical Applications: A Review," *Sensors* 19 (2019): 1706, https://doi.org/10.3390/s19071706.

31. V. Egorov, U. Gulzar, Y. Zhang, S. Breen, and C. O'Dwyer, "Evolution of 3D Printing Methods and Materials for Electrochemical Energy Storage," *Advanced Materials* 32 (2020): 2000556, https://doi.org/10.1002/adma.202000556.

32. I. J. Gómez, N. Alegret, A. Dominguez-Alfaro, and M. V. Sulleiro, "Recent Advances on 2D Materials Towards 3D Printing," *Chemistry* 3 (2021): 1314–1343, https://doi.org/10.3390/chemistry3040095.

33. K. Hassan, M. J. Nine, T. T. Tung, et al., "Functional Inks and Extrusion-Based 3D Printing of 2D Materials: A Review of Current Research and Applications," *Nanoscale* 12 (2020): 19007–19042, https://doi.org/10.1039/d0nr04933f.

34. S. S. Varghese, S. H. Varghese, S. Swaminathan, K. K. Singh, and V. Mittal, "Two-Dimensional Materials for Sensing: Graphene and Beyond," *Electronics* 4 (2015): 651–687, https://doi.org/10.3390/electronics4030651.

35. W. Choi, N. Choudhary, G. H. Han, J. Park, D. Akinwande, and Y. H. Lee, "Recent Development of Two-Dimensional Transition Metal Dichalcogenides and Their Applications," *Materials Today* 20 (2017): 116–130, https://doi.org/10.1016/j.mattod.2016.10.002.

36. C. W. Lee, J. M. Suh, and H. W. Jang, "Chemical Sensors Based on Two-Dimensional (2D) Materials for Selective Detection of Ions and Molecules in Liquid," *Frontiers in Chemistry* 7 (2019): 708, https://doi.org/10.3389/fchem.2019.00708.

37. A. Zolfagharian, A. Z. Kouzani, S. Y. Khoo, A. A. A. Moghadam, I. Gibson, and A. Kaynak, "Evolution of 3D Printed Soft Actuators,"

Sensors and Actuators A: Physical 250 (2016): 258–272, https://doi.org/10.1016/j.sna.2016.09.028.

38. L. Duan, D. R. D'hooge, and L. Cardon, "Recent Progress on Flexible and Stretchable Piezoresistive Strain Sensors: From Design to Application," *Progress in Materials Science* 114 (2020): 100617, https://doi.org/10.1016/j.pmatsci.2019.100617.

39. V. G. Rocha, E. Saiz, I. S. Tirichenko, and E. García-Tuñón, "Direct Ink Writing Advances in Multi-Material Structures for a Sustainable Future," *Journal of Materials Chemistry A* 8 (2020): 15646–15657, https://doi.org/10.1039/d0ta04181e.

40. H. Jiang, L. Zheng, Z. Liu, and X. Wang, "Two-Dimensional Materials: From Mechanical Properties to Flexible Mechanical Sensors," *InfoMat* 2 (2020): 1077–1094, https://doi.org/10.1002/inf2.12072.

41. P. V. Pham, S. C. Bodepudi, K. Shehzad, et al., "2D Heterostructures for Ubiquitous Electronics and Optoelectronics: Principles, Opportunities, and Challenges," *Chemical Reviews* 122 (2022): 6514–6613.

42. P. K. Kalambate, P. Thirabowonkitphithan, P. Kaewarsa, et al., "Progress, Challenges, and Opportunities of Two-Dimensional Layered Materials Based Electrochemical Sensors and Biosensors," *Materials Today Chemistry* 26 (2022): 101235.

43. A. Bolotsky, D. Butler, C. Dong, et al., "Two-Dimensional Materials in Biosensing and Healthcare: From In Vitro Diagnostics to Optogenetics and Beyond," *ACS Nano* 13 (2019): 9781–9810, https://doi.org/10.1021/acsnano.9b03632.

44. L. Prozorovska and P. R. Kidambi, "State-of-the-Art and Future Prospects for Atomically Thin Membranes From 2D Materials," *Advanced Materials* 30 (2018): 1801179, https://doi.org/10.1002/adma.201801179.

45. S. Zhang, S. Guo, Z. Chen, et al., "Recent Progress in 2D Group-VA Semiconductors: From Theory to Experiment," *Chemical Society Reviews* 47 (2018): 982–1021, https://doi.org/10.1039/c7cs00125h.

46. M. A. Tapia, R. Gusmão, N. Serrano, et al., "Phosphorene and Other Layered Pnictogens as a New Source of 2D Materials for Electrochemical Sensors," *TrAC Trends in Analytical Chemistry* 139 (2021): 116249, https://doi.org/10.1016/j.trac.2021.116249.

47. F. Ezzah, A. Latif, A. Numan, et al., "Evolution of MXene and its 2D Heterostructure in Electrochemical Sensor Applications," *Coordination Chemistry Reviews* 471 (2022): 214755, https://doi.org/10.1016/j.ccr.2022.214755.

48. Q. H. Wang, K. Kalantar-Zadeh, A. Kis, J. N. Coleman, and M. S. Strano, "Electronics and Optoelectronics of Two-Dimensional Transition Metal Dichalcogenides," *Nature Nanotechnology* 7 (2012): 699–712, https://doi.org/10.1038/nnano.2012.193.

49. K. F. Mak, C. Lee, J. Hone, J. Shan, and T. F. Heinz, "Atomically Thin MoS2: A New Direct-Gap Semiconductor," *Physical Review Letters* 105 (2010): 136805, https://doi.org/10.1103/PhysRevLett.105.136805.

50. A. Splendiani, L. Sun, Y. Zhang, et al., "Emerging Photoluminescence in Monolayer MoS2," *Nano Letters* 10 (2010): 1271–1275, https://doi.org/10.1021/nl903868w.

51. J. H. Zhong, J. Zhang, X. Jin, et al., "Quantitative Correlation Between Defect Density and Heterogeneous Electron Transfer Rate of Single Layer Graphene," *Journal of the American Chemical Society* 136 (2014): 16609–16617.

52. L. Zeng, L. Han, W. Nan, et al., "Regulation of Heterogeneous Electron Transfer Reactivity by Defect Engineering Through Electrochemically Induced Brominating Addition," *Chemical Science* 15 (2023): 95–101, https://doi.org/10.1039/d3sc03920j.

53. E. Cuniberto, A. Alharbi, T. Wu, et al., "Nano-Engineering the Material Structure of Preferentially Oriented Nano-Graphitic Carbon for Making High-Performance Electrochemical Micro-Sensors," *Scientific Reports* 10 (2020): 9444, https://doi.org/10.1038/s41598-020-66408-9.

54. T. Wu, A. Alharbi, R. Kiani, and D. Shahrjerdi, "Quantitative Principles for Precise Engineering of Sensitivity in Graphene Electrochemical Sensors," *Advanced Materials* 31 (2019): 1805752, https://doi.org/10.1002/adma.201805752.

55. A. G. Güell, N. Ebejer, M. E. Snowden, J. V. MacPherson, and P. R. Unwin, "Structural Correlations in Heterogeneous Electron Transfer at Monolayer and Multilayer Graphene Electrodes," *Journal of the American Chemical Society* 134 (2012): 7258–7261, https://doi.org/10.1021/ja3014902.

56. N. M. Sanches, A. Hassan, I. A. Mattioli, L. J. A. Macedo, G. C. Sedenho, and F. N. Crespilho, "Tuning Vertical Electron Transfer on Graphene Bilayer Electrochemical Devices," *Advanced Materials Interfaces* 8 (2021): 2100550, https://doi.org/10.1002/admi.202100550.

57. Y. Yu, S. Y. Huang, Y. Li, S. N. Steinmann, W. Yang, and L. Cao, "Layer-Dependent Electrocatalysis of MoS2 for Hydrogen Evolution," *Nano Letters* 14 (2014): 553–558, https://doi.org/10.1021/nl403620g.

58. H. Li, M. Du, M. J. Mleczko, et al., "Kinetic Study of Hydrogen Evolution Reaction Over Strained MoS2 With Sulfur Vacancies Using Scanning Electrochemical Microscopy," *Journal of the American Chemical Society* 138 (2016): 5123–5129, https://doi.org/10.1021/jacs.6b01377.

59. J. Ma, Z. Wang, B. Jiang, W. Wang, and H. Wang, "Directly Imaging and Regulating the Nanoscale Inhomogeneity of S-Vacancies in Molybdenum Disulfide Monolayer During Electrocatalytic Hydrogen Evolution," *Angewandte Chemie International Edition* 62 (2023): e202305846, https://doi.org/10.1002/anie.202305846.

60. Y. Wang, Y. Shao, D. W. Matson, J. Li, and Y. Lin, "Nitrogen-Doped Graphene and Its Application in Electrochemical Biosensing," *ACS Nano* 4 (2010): 1790–1798, https://doi.org/10.1021/nn100315s.

61. Y. Cao, W. Si, Y. Zhang, et al., "Nitrogen-Doped Graphene: Effect of Graphitic-N on the Electrochemical Sensing Properties Towards Acetaminophen," *FlatChem* 9 (2018): 1–7, https://doi.org/10.1016/j.flatc.2018.03.002.

62. J. Lavanya, M. Aakash, A. Ravi Sankar, and N. Gomathi, "Development of an Electrochemical Dopamine Sensor Using Nitrogen-Rich Sulfur Dual-Doped Reduced Graphene Oxide," *IEEE Access* 12 (2024): 66931–66940.

63. Z. Cai, B. Liu, X. Zou, and H. M. Cheng, "Chemical Vapor Deposition Growth and Applications of Two-Dimensional Materials and Their Heterostructures," *Chemical Reviews* 118 (2018): 6091–6133, https://doi.org/10.1021/acs.chemrev.7b00536.

64. F. R. Fan, R. Wang, H. Zhang, and W. Wu, "Emerging Beyond-Graphene Elemental 2D Materials for Energy and Catalysis Applications," *Chemical Society Reviews* 50 (2021): 10983–11031, https://doi.org/10.1039/c9cs00821g.

65. A. K. Geim and K. S. Novoselov, "The Rise of Graphene," *Nature Materials* 6 (2007): 183–191, https://doi.org/10.1038/nmat1849.

66. A. K. Geim, "Graphene: Status and Prospects," *Science* 324 (2009): 1530–1534, https://doi.org/10.1126/science.1158877.

67. M. J. Allen, V. C. Tung, and R. B. Kaner, "Honeycomb Carbon: A Review of Graphene," *Chemical Reviews* 110 (2010): 132–145, https://doi.org/10.1021/cr900070d.

68. X. Yu, H. Cheng, M. Zhang, Y. Zhao, L. Qu, and G. Shi, "Graphene-Based Smart Materials," *Nature Reviews Materials* 2 (2017): 17046, https://doi.org/10.1038/natrevmats.2017.46.

69. F. Bonaccorso, Z. Sun, T. Hasan, and A. C. Ferrari, "Graphene Photonics and Optoelectronics," *Nature Photonics* 4 (2010): 611–622, https://doi.org/10.1038/nphoton.2010.186.

70. M. V. Sulleiro, A. Dominguez-Alfaro, N. Alegret, A. Silvestri, and I. J. Gómez, "2D Materials Towards Sensing Technology: From Fundamentals to Applications," *Sensing and Bio-Sensing Research* 38 (2022): 100540, https://doi.org/10.1016/j.sbsr.2022.100540.

71. T. D. Thanh, N. D. Chuong, H. Van Hien, et al., "Recent Advances in Two-Dimensional Transition Metal Dichalcogenides-Graphene Heterostructured Materials for Electrochemical Applications," *Progress in Materials Science* 96 (2018): 51–85, https://doi.org/10.1016/j.pmatsci.2018.03.007.

72. Y. Wang, Y. Zhao, X. Ding, and L. Qiao, "Recent Advances in the Electrochemistry of Layered Post-Transition Metal Chalcogenide Nanomaterials for Hydrogen Evolution Reaction," *Journal of Energy Chemistry* 60 (2021): 451–479, https://doi.org/10.1016/j.jechem.2021.01.021.

73. J. Azadmanjiri, P. Kumar, V. K. Srivastava, and Z. Sofer, "Surface Functionalization of 2D Transition Metal Oxides and Dichalcogenides via Covalent and Non-Covalent Bonding for Sustainable Energy and Biomedical Applications," *ACS Applied Nano Materials* 3 (2020): 3116–3143, https://doi.org/10.1021/acsanm.0c00120.

74. C. Lu, Y. Liu, Y. Ying, and J. Liu, "Comparison of MoS2, WS2, and Graphene Oxide for DNA Adsorption and Sensing," *Langmuir* 33 (2017): 630–637, https://doi.org/10.1021/acs.langmuir.6b04502.

75. M. Donarelli and L. Ottaviano, "2D Materials for Gas Sensing Applications: A Review on Graphene Oxide, MoS2, WS2 and Phosphorene," *Sensors* 18 (2018): 3638, https://doi.org/10.3390/s18113638.

76. G. Oxide and M. Donarelli, "2D Materials for Gas Sensing Applications: A Review on Graphene Oxide, MoS_2, WS_2 and Phosphorene," *Sensors* 18 (2018): 3638, https://doi.org/10.3390/s18113638.

77. L. Li and Y. Zhang, "Controlling the Luminescence of Monolayer MoS2 Based on the Piezoelectric Effect," *Nano Research* 10 (2017): 2527–2534, https://doi.org/10.1007/s12274-017-1457-y.

78. S. Deng, L. Li, and M. Li, "Stability of Direct Band Gap Under Mechanical Strains for Monolayer MoS2, MoSe2, WS2 and WSe2," *Physica E: Low-Dimensional Systems and Nanostructures* 101 (2018): 44–49, https://doi.org/10.1016/j.physe.2018.03.016.

79. F. Shahzad, S. A. Zaidi, and R. A. Naqvi, "2D Transition Metal Carbides (MXene) for Electrochemical Sensing: A Review," *Critical Reviews in Analytical Chemistry* 52 (2022): 848–864, https://doi.org/10.1080/10408347.2020.1836470.

80. Y. Gogotsi and B. Anasori, "The Rise of MXenes," *ACS Nano* 13 (2019): 8491–8494, https://doi.org/10.1021/acsnano.9b06394.

81. M. Deng, J. Feng, D. Tao, et al., "A Novel Conductive Nanocomposite-Based Biosensor for Ultrasensitive Detection of microRNA-21 in Serum, Using Methylene Blue as Mediator," *Bioelectrochemistry* 148 (2022): 108256, https://doi.org/10.1016/j.bioelechem.2022.108256.

82. H. Torul, E. Yarali, E. Eksin, et al., "Paper-Based Electrochemical Biosensors for Voltammetric Detection of miRNA Biomarkers Using Reduced Graphene Oxide or MoS(2) Nanosheets Decorated With Gold Nanoparticle Electrodes," *Biosensors* 11 (2021): 236, https://doi.org/10.3390/bios11070236.

83. S. Su, W. Cao, W. Liu, et al., "Dual-Mode Electrochemical Analysis of microRNA-21 Using Gold Nanoparticle-Decorated MoS2 Nanosheet," *Biosensors and Bioelectronics* 94 (2017): 552–559, https://doi.org/10.1016/j.bios.2017.03.040.

84. Y. Lei, D. Butler, M. C. Lucking, et al., "Single-Atom Doping of MoS 2 With Manganese Enables Ultrasensitive Detection of Dopamine: Experimental and Computational Approach," *Science Advances* 6 (2020): eabc4250.

85. M. Wen, Y. Xing, G. Liu, S. Hou, and S. Hou, "Electrochemical Sensor Based on Ti(3)C(2) Membrane Doped With UIO-66-NH(2) for Dopamine," *Microchimica Acta* 189 (2022): 141, https://doi.org/10.1007/s00604-022-05222-8.

86. J. Zhao, C. He, W. Wu, et al., "MXene-MoS2 Heterostructure Collaborated With Catalyzed Hairpin Assembly for Label-Free Electrochemical Detection of microRNA-21," *Talanta* 237 (2022): 122927, https://doi.org/10.1016/j.talanta.2021.122927.

87. Y. Guo, Y. Nie, P. Wang, Z. Li, and Q. Ma, "MoS2 QDs-MXene Heterostructure-Based ECL Sensor for the Detection of miRNA-135b in Gastric Cancer Exosomes," *Talanta* 259 (2023): 124559, https://doi.org/10.1016/j.talanta.2023.124559.

88. Z. Sun, Y. Tong, L. Zhao, et al., "MoS2@Ti3C2 Nanohybrid-Based Photoelectrochemical Biosensor: A Platform for Ultrasensitive Detection of Cancer Biomarker Exosomal miRNA," *Talanta* 238 (2022): 123077, https://doi.org/10.1016/j.talanta.2021.123077.

89. J. Zheng, B. Wang, A. Ding, B. Weng, and J. Chen, "Synthesis of MXene/DNA/Pd/Pt Nanocomposite for Sensitive Detection of Dopamine," *Journal of Electroanalytical Chemistry* 816 (2018): 189–194.

90. N. Glassmaker, Y. Mi, M. Cakmak, and A. Shakouri, "Proceedings of ASME 2022 17th International Manufacturing Science and Engineering Conference," (2022) MSEC.

91. K. Maize, Y. Mi, M. Cakmak, and A. Shakouri, "Real-Time Metrology for Roll-To-Roll and Advanced Inline Manufacturing: A Review," *Advanced Materials Technologies* 8 (2023): 2200173, https://doi.org/10.1002/admt.202200173.

92. A. Amini and T. H. Gan, "A Computer Vision-Based Quality Assessment Technique for R2R Printed Silver Conductors on Flexible Plastic Substrates," *Applied Sciences* 13 (2023): 1084, https://doi.org/10.3390/app13021084.

93. L. Hakola, E. Jansson, R. Futsch, et al., "Sustainable Roll-To-Roll Manufactured Multi-Layer Smart Label," *International Journal of Advanced Manufacturing Technology* 117 (2021): 2921–2934, https://doi.org/10.1007/s00170-021-07640-z.

94. P. S. Sfragano, S. Laschi, and I. Palchetti, "Sustainable Printed Electrochemical Platforms for Greener Analytics," *Frontiers in Chemistry* 8 (2020): 8, https://doi.org/10.3389/fchem.2020.00644.

95. G. Hanrahan, D. G. Patil, and J. Wang, "Electrochemical Sensors for Environmental Monitoring: Design, Development and Applications," *Journal of Environmental Monitoring* 6 (2004): 657, https://doi.org/10.1039/b403975k.

96. D. Wei, M. J. A. Bailey, P. Andrew, and T. Ryhänen, "Electrochemical Biosensors at the Nanoscale," *Lab on a Chip* 9 (2009): 2123, https://doi.org/10.1039/b903118a.

97. R. Zeis, A. Mathur, G. Fritz, J. Lee, and J. Erlebacher, "Platinum-Plated Nanoporous Gold: An Efficient, Low pt Loading Electrocatalyst for PEM Fuel Cells," *Journal of Power Sources* 165 (2007): 65–72, https://doi.org/10.1016/j.jpowsour.2006.12.007.

98. C. Horwood, *Ionic Liquids in Analytical Chemistry: New Insights and Recent Developments* (Elsevier, 2021).

99. R. Abbel and E. R. Meinders, *Nanomaterials for 2D and 3D Printing* (Wiley, 2017).

100. J. Dai, O. Ogbeide, N. Macadam, et al., "Printed Gas Sensors," *Chemical Society Reviews* 49 (2020): 1756–1789, https://doi.org/10.1039/c9cs00459a.

101. S. M. F. Cruz, L. A. Rocha, and J. C. Viana, *Flexible Electronics* (Intech Open, 2018).

102. R. R. Søndergaard, M. Hösel, and F. C. Krebs, "Roll-To-Roll Fabrication of Large Area Functional Organic Materials," *Journal of Polymer Science, Part B: Polymer Physics* 51 (2013): 16–34, https://doi.org/10.1002/polb.23192.

103. L. W. T. Ng, G. Hu, R. C. T. Howe, et al., *Printing of Graphene and Related 2D Materials* (Springer, 2019).

104. X. Gong, K. Huang, Y. H. Wu, and X. S. Zhang, "Recent Progress on Screen-Printed Flexible Sensors for Human Health Monitoring," *Sensors and Actuators A: Physical* 345 (2022): 113821.

105. P. R. Leach, *The Printing Ink Manual* (Springer Netherlands, 1993).

106. D. Maddipatla, B. B. Narakathu, M. M. Ali, A. A. Chlaihawi, and M. Z. Atashbar, "SAS 2017–2017 IEEE Sensors Applications Symposium," (2017), Proceedings.

107. H. Kipphan, *Handbook of Print MediaHandbook of Print Media*. (Springer, 2001).

108. A. Eshkeiti, Z. Ramshani, S. Emamian, et al., "2015 IEEE SENSORS—Proceedings," (2015).

109. D. Maddipatla, B. B. Narakathu, B. J. Bazuin, and M. Z. Atashbar, "Proceedings of IEEE Sensors," (2017).

110. M. Allen, C. Lee, B. Ahn, T. Kololuoma, K. Shin, and S. Ko, "R2R Gravure and Inkjet Printed RF Resonant Tag," *Microelectronic Engineering* 88 (2011): 3293–3299, https://doi.org/10.1016/j.mee.2011.08.010.

111. P. Xue, P. Cheng, R. P. S. Han, and X. Zhan, "Printing Fabrication of Large-Area Non-Fullerene Organic Solar Cells," *Materials Horizons* 9 (2022): 194–219, https://doi.org/10.1039/d1mh01317c.

112. H. Zhang, A. Ramm, S. Lim, et al., "Wettability Contrast Gravure Printing," *Advanced Materials* 27 (2015): 7420–7425, https://doi.org/10.1002/adma.201502639.

113. G. Hu, J. Kang, L. W. T. Ng, et al., "Functional Inks and Printing of Two-Dimensional Materials," *Chemical Society Reviews* 47 (2018): 3265–3300, https://doi.org/10.1039/c8cs00084k.

114. R. C. Kattumenu, "ProQuest Dissertations and Theses," (2008).

115. T. Mäkelä, T. Haatainen, P. Majander, and J. Ahopelto, "Continuous Roll to Roll Nanoimprinting of Inherently Conducting Polyaniline," *Microelectronic Engineering* 84 (2007): 877–879, https://doi.org/10.1016/j.mee.2007.01.131.

116. P. Kopola, M. Tuomikoski, R. Suhonen, and A. Maaninen, "Gravure Printed Organic Light Emitting Diodes for Lighting Applications," *Thin Solid Films* 517 (2009): 5757–5762, https://doi.org/10.1016/j.tsf.2009.03.209.

117. D. Deganello, J. A. Cherry, D. T. Gethin, and T. C. Claypole, "Patterning of Micro-Scale Conductive Networks Using Reel-To-Reel Flexographic Printing," *Thin Solid Films* 518 (2010): 6113–6116, https://doi.org/10.1016/j.tsf.2010.05.125.

118. R. Faddoul, N. Reverdy-Bruas, A. Blayo, T. Haas, and C. Zeilmann, "Optimisation of Silver Paste for Flexography Printing on LTCC Substrate," *Microelectronics Reliability* 52 (2012): 1483–1491.

119. A. Mujahid, N. Iqbal, and A. Afzal, "Bioimprinting Strategies: From Soft Lithography to Biomimetic Sensors and Beyond," *Biotechnology Advances* 31 (2013): 1435–1447, https://doi.org/10.1016/j.biotechadv.2013.06.008.

120. Y. Huang, H. Wu, L. Xiao, et al., "Assembly and Applications of 3D Conformal Electronics on Curvilinear Surfaces," *Materials Horizons* 6 (2019): 642–683, https://doi.org/10.1039/c8mh01450g.

121. G. M. Whitesides, E. Ostuni, S. Takayama, X. Jiang, and D. E. Ingber, "Soft Lithography in Biology and Biochemistry," *Annual Review of Biomedical Engineering* 3 (2001): 335–373, https://doi.org/10.1146/annurev.bioeng.3.1.335.

122. D. A. Ferreira, M. Rothbauer, J. P. Conde, P. Ertl, C. Oliveira, and P. L. Granja, "A Fast Alternative to Soft Lithography for the Fabrication of Organ-On-a-Chip Elastomeric-Based Devices and Microactuators," *Advanced Science* 8 (2021): 8, https://doi.org/10.1002/advs.202003273.

123. N. C. Raut and K. Al-Shamery, "Inkjet Printing Metals on Flexible Materials for Plastic and Paper Electronics," *Journal of Materials Chemistry C* 6 (2018): 1618–1641, https://doi.org/10.1039/c7tc04804a.

124. S. K. Karunakaran, G. M. Arumugam, W. Yang, et al., "Recent Progress in Inkjet-Printed Solar Cells," *Journal of Materials Chemistry A* 7 (2019): 13873–13902, https://doi.org/10.1039/c9ta03155c.

125. Y. J. Heo, S. Iwanaga, and S. Takeuchi, "Proceedings of the IEEE International Conference on Micro Electro Mechanical Systems (MEMS)," (2012).

126. H. Zhang, S. K. Moon, and T. H. Ngo, "3D Printed Electronics of Non-Contact Ink Writing Techniques: Status and Promise," *International Journal of Precision Engineering and Manufacturing - Green Technology* 7 (2020): 511–524, https://doi.org/10.1007/s40684-019-00139-9.

127. I. Reinhold, "Inkjet Printing of Functional Materials and Post-Processing," In *Nanomaterials for 2D and 3D Printing*, edited by S. Magdassi, and A. Kamyshny (Wiley-VCH, 2017), 27–49, https://doi.org/10.1002/9783527685790.ch2.

128. R. GmbH, "Inkjet—Printing Without Touch," https://www.ruhlamat.com/en/wiki/inkjet-printing-without-touch#:~:text=Inkjet%20is%20a%20modern%20printing,the%20object%20to%20be%20printed.

129. X. Luo, "Application of Inkjet-Printing Technology in Developing Indicators/Sensors for Intelligent Packaging Systems," *Current Opinion in Food Science* 46 (2022): 100868.

130. M. M. Mohebi and J. R. G. Evans, "A Drop-On-Demand Ink-Jet Printer for Combinatorial Libraries and Functionally Graded Ceramics," *Journal of Combinatorial Chemistry* 4 (2002): 267–274, https://doi.org/10.1021/cc010075e.

131. B. Derby, "Inkjet Printing of Functional and Structural Materials: Fluid Property Requirements, Feature Stability, and Resolution," *Annual Review of Materials Research* 40 (2010): 395–414, https://doi.org/10.1146/annurev-matsci-070909-104502.

132. H. Maleki and V. Bertola, "Recent Advances and Prospects of Inkjet Printing in Heterogeneous Catalysis," *Catalysis Science and Technology* 10 (2020): 3140–3159, https://doi.org/10.1039/d0cy00040j.

133. H. W. Tan, T. Tran, and C. K. Chua, "A Review of Printed Passive Electronic Components Through Fully Additive Manufacturing Methods," *Virtual and Physical Prototyping* 11 (2016): 271–288, https://doi.org/10.1080/17452759.2016.1217586.

134. D. E. Kravchenko, A. Matavž, V. Rubio-Giménez, H. Vanduffel, M. Verstreken, and R. Ameloot, "Aerosol Jet Printing of the Ultramicroporous Calcium Squarate Metal–Organic Framework," *Chemistry of Materials* 34 (2022): 6809–6814.

135. Y. Wu, A. Lin, J. Zhang, et al., "Aerosol Jet Printing of Hybrid Ti3C2Tx/C Nanospheres for Planar Micro-Supercapacitors," *Frontiers in Chemistry* 10 (2022): 1.

136. S. Binder, M. Glatthaar, and E. Rädlein, "Analytical Investigation of Aerosol Jet Printing," *Aerosol Science and Technology* 48 (2014): 924–929, https://doi.org/10.1080/02786826.2014.940439.

137. N. X. Williams, S. Noyce, J. A. Cardenas, B. J. Wiley, and A. D. Franklin, "Silver Nanowire Inks for Direct-Write Electronic Tattoo Applications," *Nanoscale* 11 (2019): 14294–14302, https://doi.org/10.1039/c9nr03378e.

138. S. Lu and A. D. Franklin, "Printed Carbon Nanotube Thin-Film Transistors: Progress on Printable Materials and the Path to Applications," *Nanoscale* 12 (2020): 23371–23390, https://doi.org/10.1039/d0nr06231f.

139. E. B. Secor, "Principles of Aerosol Jet Printing," *Flexible and Printed Electronics* 3 (2018): 35002, https://doi.org/10.1088/2058-8585/aace28.

140. M. Wang, Q. Liu, H. Zhang, et al., "Laser Direct Writing of Tree-Shaped Hierarchical Cones on a Superhydrophobic Film for High-Efficiency Water Collection," *ACS Applied Materials and Interfaces* 9 (2017): 29248–29254, https://doi.org/10.1021/acsami.7b08116.

141. X. Wang and Q. Zhang, "Recent Progress on Laser Fabrication of On-Chip Microsupercapacitors," *Journal of Energy Storage* 34 (2021): 101994, https://doi.org/10.1016/j.est.2020.101994.

142. S. Wang, Z. Zhou, B. Li, C. Wang, and Q. Liu, "Progresses on New Generation Laser Direct Writing Technique," *Materials Today Nano* 16 (2021): 100142, https://doi.org/10.1016/j.mtnano.2021.100142.

143. Y. Ni, R. Ji, K. Long, T. Bu, K. Chen, and S. Zhuang, "A Review of 3D-Printed Sensors," *Applied Spectroscopy Reviews* 52 (2017): 623–652, https://doi.org/10.1080/05704928.2017.1287082.

144. T. Rayna and L. Striukova, "From Rapid Prototyping to Home Fabrication: How 3D Printing Is Changing Business Model Innovation," *Technological Forecasting and Social Change* 102 (2016): 214–224, https://doi.org/10.1016/j.techfore.2015.07.023.

145. E. MacDonald, R. Salas, D. Espalin, et al., "3D Printing for the Rapid Prototyping of Structural Electronics," *IEEE Access* 2 (2014): 234–242, https://doi.org/10.1109/ACCESS.2014.2311810.

146. I. J. Petrick and T. W. Simpson, "3D Printing Disrupts Manufacturing: How Economies of One Create New Rules of Competition," *Research-Technology Management* 56 (2013): 12–16, https://doi.org/10.5437/08956308X5606193.

147. A. Naderi, N. Bhattacharjee, and A. Folch, "Digital Manufacturing for Microfluidics," *Annual Review of Biomedical Engineering* 21 (2019): 325–364, https://doi.org/10.1146/annurev-bioeng-092618-020341.

148. H. K. Balakrishnan, F. Badar, E. H. Doeven, et al., "3D Printing: An Alternative Microfabrication Approach With Unprecedented Opportunities in Design," *Analytical Chemistry* 93 (2021): 350–366, https://doi.org/10.1021/acs.analchem.0c04672.

149. A. Abdalla and B. A. Patel, "3D Printed Electrochemical Sensors," *Annual Review of Analytical Chemistry* 14 (2021): 47–63, https://doi.org/10.1146/annurev-anchem-091120-093659.

150. E. MacDonald and R. Wicker, "Multiprocess 3D Printing for Increasing Component Functionality," *Science* 353 (2016): aaf2093, https://doi.org/10.1126/science.aaf2093.

151. Z. Huang, G. Shao, and L. Li, "Micro/Nano Functional Devices Fabricated by Additive Manufacturing," *Progress in Materials Science* 131 (2023): 101020.

152. R. L. Truby and J. A. Lewis, "Printing Soft Matter in Three Dimensions," *Nature* 540 (2016): 371–378, https://doi.org/10.1038/nature21003.

153. A. Abdalla and B. A. Patel, "3D-Printed Electrochemical Sensors: A New Horizon for Measurement of Biomolecules," *Current Opinion in Electrochemistry* 20 (2020): 78–81, https://doi.org/10.1016/j.coelec.2020.04.009.

154. M. P. Browne, E. Redondo, and M. Pumera, "3D Printing for Electrochemical Energy Applications," *Chemical Reviews* 120 (2020): 2783–2810, https://doi.org/10.1021/acs.chemrev.9b00783.

155. L. J. G. Ouedraogo, M. Kling, and N. N. Hashemi, "Graphene Microelectrodes for Real-Time Impedance Spectroscopy of Neural Cells in Organ-On-a-Chip," *APL Materials* 13 (2025): 21113, https://doi.org/10.1063/5.0252728.

156. W. B. Veloso, T. R. L. C. Paixao, and G. N. Meloni, "The Current Shortcomings and Future Possibilities of 3D Printed Electrodes," *Analytical Chemistry* 96 (2024): 14315–14319.

157. R. S. Shergill and B. A. Patel, "The Effects of Material Extrusion Printing Speed on the Electrochemical Activity of Carbon Black/Polylactic Acid Electrodes**," *ChemElectroChem* 9 (2022): e202200831, https://doi.org/10.1002/celc.202200831.

158. W. J. Scheideler and J. Im, "Recent Advances in 3D Printed Electrodes–Bridging the Nano to Mesoscale," *Advanced Science* 12 (2025): 12, https://doi.org/10.1002/advs.202411951.

159. H. Yamada, H. Nakamura, F. Nakahara, I. Moriguchi, and T. Kudo, "Electrochemical Study of High Electrochemical Double Layer Capacitance of Ordered Porous Carbons With Both Meso/Macropores and Micropores," *Journal of Physical Chemistry C* 111 (2007): 227–233, https://doi.org/10.1021/jp063902g.

160. D. P. Rocha, R. G. Rocha, S. V. F. Castro, et al., "Posttreatment of 3D-Printed Surfaces for Electrochemical Applications: A Critical Review on Proposed Protocols," *Electrochemical Science Advances* 2 (2022): e2100136, https://doi.org/10.1002/elsa.202100136.

161. Y. Zhou, X. Xia, X. Liu, et al., "Preparation and Rheological and Mechanical Properties of Poly(Butylene Succinate)/talc Composites for Material Extrusion Additive Manufacturing," *Macromolecular Materials and Engineering* 304 (2019): 1900021, https://doi.org/10.1002/mame.201900021.

162. R. M. Cardoso, C. Kalinke, R. G. Rocha, et al., "Additive-Manufactured (3D-Printed) Electrochemical Sensors: A Critical Review," In *Analytica Chimica Acta*, edited by S. Magdassi, and A. Kamyshny, vol. 1118 (Wiley-VCH, 2017), 27–49, https://doi.org/10.1016/j.aca.2020.03.028.

163. M. A. Ali, C. Hu, E. A. Yttri, and R. Panat, "Recent Advances in 3D Printing of Biomedical Sensing Devices," *Advanced Functional Materials* 32 (2022): 2107671, https://doi.org/10.1002/adfm.202107671.

164. A. K. Pal, A. K. Mohanty, and M. Misra, "Additive Manufacturing Technology of Polymeric Materials for Customized Products: Recent Developments and Future Prospective," *RSC Advances* 11 (2021): 36398–36438, https://doi.org/10.1039/d1ra04060j.

165. B. Gross, S. Y. Lockwood, and D. M. Spence, "Recent Advances in Analytical Chemistry by 3D Printing," *Analytical Chemistry* 89 (2017): 57–70, https://doi.org/10.1021/acs.analchem.6b04344.

166. M. Criado-Gonzalez, A. Dominguez-Alfaro, N. Lopez-Larrea, N. Alegret, and D. Mecerreyes, "Additive Manufacturing of Conducting Polymers: Recent Advances, Challenges, and Opportunities," *ACS Applied Polymer Materials* 3 (2021): 2865–2883, https://doi.org/10.1021/acsapm.1c00252.

167. M. Colaco, D. A. Igel, and A. Atala, "The Potential of 3D Printing in Urological Research and Patient Care," *Nature Reviews Urology* 15 (2018): 213–221, https://doi.org/10.1038/nrurol.2018.6.

168. K. Zub, S. Hoeppener, and U. S. Schubert, "Inkjet Printing and 3D Printing Strategies for Biosensing, Analytical, and Diagnostic Applications," *Advanced Materials* 34 (2022): 2105015, https://doi.org/10.1002/adma.202105015.

169. S. Vadodaria and T. Mills, "Jetting-Based 3D Printing of Edible Materials," *Food Hydrocolloids* 106 (2020): 105857, https://doi.org/10.1016/j.foodhyd.2020.105857.

170. E. A. Clark, M. R. Alexander, D. J. Irvine, et al., "3D Printing of Tablets Using Inkjet With UV Photoinitiation," *International Journal of Pharmaceutics* 529 (2017): 523–530, https://doi.org/10.1016/j.ijpharm.2017.06.085.

171. C. Sturgess, C. J. Tuck, I. A. Ashcroft, and R. D. Wildman, "3D Reactive Inkjet Printing of Polydimethylsiloxane," *Journal of Materials Chemistry C* 5 (2017): 9733–9743, https://doi.org/10.1039/c7tc02412f.

172. T. Wang, C. Zhou, and W. Xu, "Online Droplet Monitoring in Inkjet 3D Printing Using Catadioptric Stereo System," *IISE Transactions* 51 (2019): 153–167, https://doi.org/10.1080/24725854.2018.1532133.

173. H. Wang, J. Wang, J. Tao, K. Jin, and Y. Li, "3D Printing and Freeze Casting Hierarchical Mxene Pressure Sensor," *Nano* 10 (2024): 68–77, https://doi.org/10.1080/20550324.2023.2291626.

174. S. W. Lee, X. Pei, J. Rajendran, and R. Esfandyarpour, "A Wireless and Battery-Free Wearable Pressure Sensing System for Human–Machine Interaction and Health Monitoring," *IEEE Journal on Flexible Electronics* 2 (2023): 439–447, https://doi.org/10.1109/JFLEX.2023.3300997.

175. J. Yang, K. Ling, L. Liu, et al., "Printable and Wearable Graphene-Based Strain Sensor With High Sensitivity for Human Motion

Monitoring," *IEEE Sensors Journal* 22 (2022): 13937–13944, https://doi.org/10.1109/JSEN.2022.3180081.

176. S. Sharma, A. Chhetry, M. Sharifuzzaman, H. Yoon, and J. Y. Park, "Wearable Capacitive Pressure Sensor Based on MXene Composite Nanofibrous Scaffolds for Reliable Human Physiological Signal Acquisition," *ACS Applied Materials and Interfaces* 12 (2020): 22212–22224, https://doi.org/10.1021/acsami.0c05819.

177. A. Saleh, S. Wustoni, E. Bihar, et al., "Inkjet-Printed Ti3C2Tx MXene Electrodes for Multimodal Cutaneous Biosensing," *Journal of Physics: Materials* 3 (2020): 44004, https://doi.org/10.1088/2515-7639/abb361.

178. M. Askari, M. Afzali Naniz, M. Kouhi, A. Saberi, A. Zolfagharian, and M. Bodaghi, "Recent Progress in Extrusion 3D Bioprinting of Hydrogel Biomaterials for Tissue Regeneration: A Comprehensive Review With Focus on Advanced Fabrication Techniques," *Biomaterials Science* 9 (2021): 535–573, https://doi.org/10.1039/d0bm00973c.

179. S. H. Park, R. Su, J. Jeong, et al., "3D Printed Polymer Photodetectors," *Advanced Materials* 30 (2018): 1803980, https://doi.org/10.1002/adma.201803980.

180. C. C. Chang, E. D. Boland, S. K. Williams, and J. B. Hoying, "Direct-Write Bioprinting Three-Dimensional Biohybrid Systems for Future Regenerative Therapies," *Journal of Biomedical Materials Research. Part B, Applied Biomaterials* 98 (2011): 160–170, https://doi.org/10.1002/jbm.b.31831.

181. K. Jakab, B. Damon, A. Neagu, A. Kachurin, and G. Forgacs, "Three-Dimensional Tissue Constructs Built by Bioprinting," *Biorheolog* 43, no. 3-4 (2006): 509–513, https://doi.org/10.1177/0006355X2006043003004033.

182. T. Agarwal, M. Costantini, and T. K. Maiti, "Extrusion 3D Printing With Pectin-Based Ink Formulations: Recent Trends in Tissue Engineering and Food Manufacturing," *Biomedical Engineering Advances* 2 (2021): 100018, https://doi.org/10.1016/j.bea.2021.100018.

183. H. H. Hwang, W. Zhu, G. Victorine, N. Lawrence, and S. Chen, "3D-Printing of Functional Biomedical Microdevices via Light- and Extrusion-Based Approaches," *Small Methods* 2 (2018): 2, https://doi.org/10.1002/smtd.201700277.

184. P. K. Chakraborty, J. Azadmanjiri, C. L. P. Pavithra, et al., "Advancements in Therapeutics via 3D Printed Multifunctional Architectures From Dispersed 2D Nanomaterial Inks," *Small* 16 (2020): 2004900, https://doi.org/10.1002/smll.202004900.

185. E. Sanchez-Rexach, T. G. Johnston, C. Jehanno, H. Sardon, and A. Nelson, "Sustainable Materials and Chemical Processes for Additive Manufacturing," *Chemistry of Materials* 32 (2020): 7105–7119, https://doi.org/10.1021/acs.chemmater.0c02008.

186. D. Ahn, L. M. Stevens, K. Zhou, and Z. A. Page, "Rapid High-Resolution Visible Light 3D Printing," *ACS Central Science* 6 (2020): 1555–1563, https://doi.org/10.1021/acscentsci.0c00929.

187. D. Ravichandran, W. Xu, S. Jambhulkar, et al., "Intrinsic Field-Induced Nanoparticle Assembly in Three-Dimensional (3D) Printing Polymeric Composites," *ACS Applied Materials and Interfaces* 13 (2021): 52274–52294, https://doi.org/10.1021/acsami.1c12763.

188. J. Feng, B. L. Su, H. Xia, et al., "Printed Aerogels: Chemistry, Processing, and Applications," *Chemical Society Reviews* 50 (2021): 3842–3888, https://doi.org/10.1039/c9cs00757a.

189. Y. Wu, H. Su, M. Li, and H. Xing, "Digital Light Processing-Based Multi-Material Bioprinting: Processes, Applications, and Perspectives," *Journal of Biomedical Materials Research* 111, no. 4 (2023): 527–542, https://doi.org/10.1002/jbm.a.37473.

190. Y. Bao, "Recent Trends in Advanced Photoinitiators for Vat Photopolymerization 3D Printing," *Macromolecular Rapid Communications* 43 (2022): 1, https://doi.org/10.1002/marc.202200202.

191. J. Li, C. Boyer, and X. Zhang, "3D Printing Based on Photopolymerization and Photocatalysts: Review and Prospect," *Macromolecular Materials and Engineering* 307 (2022): 1.

192. J. S. Stefano, C. Kalinke, R. G. Da Rocha, et al., "Electrochemical (Bio)sensors Enabled by Fused Deposition Modeling-Based 3D Printing: A Guide to Selecting Designs, Printing Parameters, and Post-Treatment Protocols," *Analytical Chemistry* 94 (2022): 6417–6429, https://doi.org/10.1021/acs.analchem.1c05523.

193. S. Tajik, C. N. Garcia, S. Gillooley, and L. Tayebi, "3D Printing of Hybrid-Hydrogel Materials for Tissue Engineering: A Critical Review," *Regenerative Engineering and Translational Medicine* 9 (2023): 29–41, https://doi.org/10.1007/s40883-022-00267-w.

194. S. G. Marapureddy, P. Hivare, A. Sharma, et al., "Rheology and Direct Write Printing of Chitosan," *Carbohydrate Polymers* 269 (2021): 118254, https://doi.org/10.1016/j.carbpol.2021.118254.

195. G. Zhou, M. C. Li, C. Liu, C. Liu, Z. Li, and C. Mei, "3D Printed Nitrogen-Doped Thick Carbon Architectures for Supercapacitor: Ink Rheology and Electrochemical Performance," *Advanced Science* 10 (2023): 2206320, https://doi.org/10.1002/advs.202206320.

196. J. Li, X. Liu, J. M. Crook, and G. G. Wallace, "Development of 3D Printable Graphene Oxide Based Bio-Ink for Cell Support and Tissue Engineering," *Frontiers in Bioengineering and Biotechnology* 10 (2022): 10, https://doi.org/10.3389/fbioe.2022.994776.

197. E. Erfanian, M. Goodarzi, G. Banvillet, et al., "Additive-Free Graphene-Based Inks for 3D Printing Functional Conductive Aerogels," *Journal of Materials Chemistry A* 12 (2024): 25715.

198. X. Yun, B. Lu, Z. Xiong, et al., "Direct 3D Printing of a Graphene Oxide Hydrogel for Fabrication of a High Areal Specific Capacitance Microsupercapacitor," *RSC Advances* 9 (2019): 29384–29395, https://doi.org/10.1039/c9ra04882k.

199. G. Zhou, M. C. Li, C. Liu, Q. Wu, and C. Mei, "3D Printed Ti3C2Tx MXene/Cellulose Nanofiber Architectures for Solid-State Supercapacitors: Ink Rheology, 3D Printability, and Electrochemical Performance," *Advanced Functional Materials* 32 (2022): 2109593, https://doi.org/10.1002/adfm.202109593.

200. R. Su, F. Wang, and M. C. McAlpine, "3D Printed Microfluidics: Advances in Strategies, Integration, and Applications," *Lab on a Chip* 23 (2023): 1279–1299, https://doi.org/10.1039/d2lc01177h.

201. D. Jang, D. Kim, and J. Moon, "Influence of Fluid Physical Properties on Ink-Jet Printability," *Langmuir* 25 (2009): 2629–2635, https://doi.org/10.1021/la900059m.

202. P. J. Smith and A. Morrin, *Reactive Inkjet Printing: A Chemical Synthesis Tool* (Royal Society of Chemistry, 2017).

203. A. Hussain, N. Abbas, and A. Ali, "Inkjet Printing: A Viable Technology for Biosensor Fabrication," *Chem* 10 (2022): 103, https://doi.org/10.3390/chemosensors10030103.

204. L. Zeng, S. Ling, D. Du, H. He, X. Li, and C. Zhang, "Direct Ink Writing 3D Printing for High-Performance Electrochemical Energy Storage Devices: A Minireview," *Advanced Science* 10 (2023): 10, https://doi.org/10.1002/advs.202303716.

205. V. F. Paz, M. Emons, K. Obata, et al., "Development of Functional Sub-100 Nm Structures With 3D Two-Photon Polymerization Technique and Optical Methods for Characterization," *Journal of Laser Applications* 24 (2012): 042004, https://doi.org/10.2351/1.4712151.

206. X. Jing, H. Fu, B. Yu, M. Sun, and L. Wang, "Two-Photon Polymerization for 3D Biomedical Scaffolds: Overview and Updates," *Frontiers in Bioengineering and Biotechnology* 10 (2022): 10, https://doi.org/10.3389/fbioe.2022.994355.

207. F. Zhang, L. Zhu, Z. Li, et al., "The Recent Development of Vat Photopolymerization: A Review," *Additive Manufacturing* 48 (2021): 102423, https://doi.org/10.1016/j.addma.2021.102423.

208. H. Shafique, V. Karamzadeh, G. Kim, et al., "High-Resolution Low-Cost LCD 3D Printing for Microfluidics and Organ-On-a-Chip Devices," *Lab on a Chip* 24 (2024): 2774–2790.

209. V. Beedasy and P. J. Smith, "Printed Electronics as Prepared by Inkjet Printing," *Materials* 13 (2020): 13, https://doi.org/10.3390/ma13030704.

210. J. Haas, F. Ulrich, C. Hofer, X. Wang, K. Braun, and J. C. Meyer, "Aligned Stacking of Nanopatterned 2D Materials for High-Resolution 3D Device Fabrication," *ACS Nano* 16 (2022): 1836–1846, https://doi.org/10.1021/acsnano.1c09122.

211. H. Zhou, H. Yang, S. Yao, L. Jiang, N. Sun, and H. Pang, "Synthesis of 3D Printing Materials and Their Electrochemical Applications," *Chinese Chemical Letters* 33 (2022): 3681–3694, https://doi.org/10.1016/j.cclet.2021.11.018.

212. S. Falina, K. Anuar, S. A. Shafiee, et al., "Two-Dimensional Non-Carbon Materials-Based Electrochemical Printed Sensors: An Updated Review," *Sensors* 22 (2022): 22, https://doi.org/10.3390/s22239358.

213. S. Pinilla, J. Coelho, K. Li, J. Liu, and V. Nicolosi, "Two-Dimensional Material Inks," *Nature Reviews Materials* 7 (2022): 717–735.

214. K. L. Ng, B. M. Maciejewska, L. Qin, et al., "Direct Evidence of the Exfoliation Efficiency and Graphene Dispersibility of Green Solvents Toward Sustainable Graphene Production," *ACS Sustainable Chemistry and Engineering* 11 (2023): 58–66, https://doi.org/10.1021/acssuschemeng.2c03594.

215. G. Hu, L. Yang, Z. Yang, et al., "A General Ink Formulation of 2D Crystals for Wafer-Scale Inkjet Printing," *Science Advances* 6 (2020): 6, https://doi.org/10.1126/sciadv.aba5029.

216. R. Narayan and S. O. Kim, "Surfactant Mediated Liquid Phase Exfoliation of Graphene," *Nano Convergence* 2 (2015): 20, https://doi.org/10.1186/s40580-015-0050-x.

217. X. Li, M. Jamali, and L. A. Fielding, "Pyrene-Functionalized Poly(Methacrylic Acid) Acts as an Efficient Stabilizer for Graphene Nanoplatelets and Facilitates Their Use in Waterborne Latex Formulations," *Journal of Colloid and Interface Science* 676 (2024): 396–407.

218. Z. Aghayar, M. Malaki, and Y. Zhang, "MXene-Based Ink Design for Printed Applications," *Nanomaterials* 12 (2022): 12, https://doi.org/10.3390/nano12234346.

219. H. Y. Jun, S. J. Kim, and C. H. Choi, "Ink Formulation and Printing Parameters for Inkjet Printing of Two Dimensional Materials: A Mini Review," *Nanomaterials* 11 (2021): 11, https://doi.org/10.3390/nano11123441.

220. R. Kaindl, T. Gupta, A. Blümel, et al., "Aerosol Jet Printing of Graphene and Carbon Nanotube Patterns on Realistically Rugged Substrates," *ACS Omega* 6 (2021): 34301–34313, https://doi.org/10.1021/acsomega.1c03871.

221. G. E. S. Garcia, R. R. de Sousa Junior, J. R. Gouveia, and D. J. dos Santos, "Graphene Oxide-Based Nanocomposites for Stereolithography (SLA) 3D Printing: Comprehensive Mechanical Characterization Under Combined Loading Modes," *Polymers* 16 (2024): 1261, https://doi.org/10.3390/polym16091261.

222. T. Sheikh and K. Behdinan, "Fused Deposition Modelling of Thermoplastic Polymer Nanocomposites: A Critical Review," *C* 10 (2024): 29, https://doi.org/10.3390/c10020029.

223. A. Lee, M. Shekhirev, M. Anayee, and Y. Gogotsi, "Multi-Year Study of Environmental Stability of Ti3C2Tx MXene Films," *Graphene and 2D Materials* 9 (2024): 77–85.

224. A. Chae, G. Murali, S. Y. Lee, et al., "Highly Oxidation-Resistant and Self-Healable MXene-Based Hydrogels for Wearable Strain Sensor," *Advanced Functional Materials* 33 (2023): 2213382, https://doi.org/10.1002/adfm.202213382.

225. Z. Wang, X. Zou, Z. Yang, et al., "Highly Sensitive Temperature Detection Based on a Frost- and Dehydration-Resistive Ion-Doped Hydrogel-MXene Composite," *ACS Applied Materials and Interfaces* 15 (2023): 35525–35533, https://doi.org/10.1021/acsami.3c06581.

226. K. Chen, W. Lai, W. Xiao, L. Li, S. Huang, and X. Xiao, "Low-Temperature Adaptive Dual-Network MXene Nanocomposite Hydrogel as Flexible Wearable Strain Sensors," *Micromachines (Basel)* 14 (2023): 14, https://doi.org/10.3390/mi14081563.

227. R. Yang, J. Zhou, C. Yang, L. Qiu, and H. Cheng, "Recent Progress in 3D Printing of 2D Material-Based Macrostructures," *Advanced Materials Technologies* 5 (2020): 1901066, https://doi.org/10.1002/admt.201901066.

228. Y. Lei, T. Zhang, Y. C. Lin, et al., "Graphene and Beyond: Recent Advances in Two-Dimensional Materials Synthesis, Properties, and Devices," *ACS Nanoscience Au* 2 (2022): 450–485, https://doi.org/10.1021/acsnanoscienceau.2c00017.

229. V. Nicolosi, M. Chhowalla, M. G. Kanatzidis, M. S. Strano, and J. N. Coleman, "Liquid Exfoliation of Layered Materials," *Science* 2013 (1979): 340, https://doi.org/10.1126/science.1226419.

230. X. Tian, J. Jin, S. Yuan, C. K. Chua, S. B. Tor, and K. Zhou, "Emerging 3D-Printed Electrochemical Energy Storage Devices: A Critical Review," *Advanced Energy Materials* 7 (2017): 1700127, https://doi.org/10.1002/aenm.201700127.

231. A. C. Bressi, A. Dallinger, Y. Steksova, and F. Greco, "Bioderived Laser-Induced Graphene for Sensors and Supercapacitors," *ACS Applied Materials and Interfaces* 15 (2023): 35788–35814, https://doi.org/10.1021/acsami.3c07687.

232. A. Adiraju, A. Jalasutram, A. Al-Hamry, et al., "Laser-Induced Fibers and Copper Phthalocyanine Modified Laser-Induced Graphene Electrodes for Sensitive and Selective Electrochemical Detection of Nitrite," *RSC Advances* 14 (2024): 28648–28658.

233. R. D. Crapnell, A. G. M. Ferrari, N. C. Dempsey, and C. E. Banks, "Electroanalytical Overview: Screen-Printed Electrochemical Sensing Platforms for the Detection of Vital Cardiac, Cancer and Inflammatory Biomarkers," *Sensors and Diagnostics* 1 (2022): 405–428, https://doi.org/10.1039/d1sd00041a.

234. S. Lakard, I. A. Pavel, and B. Lakard, "Electrochemical Biosensing of Dopamine Neurotransmitter: A Review," *Biosensors-Basel* 11 (2021): 11, https://doi.org/10.3390/bios11060179.

235. M. A. S. R. Saadi, A. Maguire, N. T. Pottackal, et al., "Direct Ink Writing: A 3D Printing Technology for Diverse Materials," *Advanced Materials* 34 (2022): 2108855, https://doi.org/10.1002/adma.202108855.

236. N. W. Pu, C. A. Wang, Y. M. Liu, Y. Sung, D. S. Wang, and M. Der Ger, "Dispersion of Graphene in Aqueous Solutions With Different Types of Surfactants and the Production of Graphene Films by Spray or Drop Coating," *Journal of the Taiwan Institute of Chemical Engineers* 43 (2012): 140–146, https://doi.org/10.1016/j.jtice.2011.06.012.

237. S. C. Ray, *Applications of Graphene and Graphene-Oxide Based Nanomaterials* (William Andrew (Elsevier), 2015).

238. T. F. Emiru and D. W. Ayele, "Controlled Synthesis, Characterization and Reduction of Graphene Oxide: A Convenient Method for Large Scale Production," *Egyptian Journal of Basic and Applied Sciences* 4 (2017): 74–79, https://doi.org/10.1016/j.ejbas.2016.11.002.

239. M. A. Ali, C. Hu, S. Jahan, et al., "Advanced Materials," 33 (2021), https://doi.org/10.1002/adma.202006647.

240. A. Sanati, E. Bidram, A. Poursamar, M. Rabbani, and M. Rafienia, "Water-Based Chitosan/Reduced Graphene Oxide Ink for Extrusion Printing of a Disposable Amperometric Glucose Sensor," *FlatChem* 36 (2022): 100443.

241. J. S. Stefano, L. R. Guterres e Silva, R. G. Rocha, et al., "New Conductive Filament Ready-To-Use for 3D-Printing Electrochemical

(Bio)sensors: Towards the Detection of SARS-CoV-2," *Analytica Chimica Acta* 1191 (2022): 339372, https://doi.org/10.1016/j.aca.2021.339372.

242. C. L. Manzanares Palenzuela, F. Novotný, P. Krupička, Z. Sofer, and M. Pumera, "Anal Chem," 90 (2018), https://doi.org/10.1021/acs.analchem.8b00083.

243. V. Katic, P. L. Dos Santos, M. F. Dos Santos, et al., "3D Printed Graphene Electrodes Modified With Prussian Blue: Emerging Electrochemical Sensing Platform for Peroxide Detection," *ACS Applied Materials and Interfaces* 11 (2019): 35068–35078, https://doi.org/10.1021/acsami.9b09305.

244. G. L. D. Estadulho, L. M. Alencar, K. E. Guima, M. A. G. Trindade, and C. A. Martins, "3D-Printed Templates Converted Into Graphite, Ruthenium, or Copper Are Used as Monolithic Sensors," *ACS Applied Electronic Materials* 3 (2021): 3482–3488, https://doi.org/10.1021/acsaelm.1c00437.

245. J. G. Walters, S. Ahmed, I. M. Terrero Rodríguez, and G. D. O'Neil, "Trace Analysis of Heavy Metals (Cd, pb, hg) Using Native and Modified 3D Printed Graphene/Poly(Lactic Acid) Composite Electrodes," *Electroanalysis* 32 (2020): 859–866, https://doi.org/10.1002/elan.201900658.

246. K. Hassan, T. T. Tung, N. Stanley, et al., "Graphene Ink for 3D Extrusion Micro Printing of Chemo-Resistive Sensing Devices for Volatile Organic Compound Detection," *Nanoscale* 13 (2021): 5356–5368.

247. Z. Zhang, Y. Zhao, Z. Zhao, G. Huang, and Y. Mei, "Atomic Layer Deposition-Derived Nanomaterials: Oxides, Transition Metal Dichalcogenides, and Metal–Organic Frameworks," *Chemistry of Materials* 32 (2020): 9056–9077, https://doi.org/10.1021/acs.chemmater.9b04414.

248. H. L. Zhuang and R. G. Hennig, "Computational Search for Single-Layer Transition-Metal Dichalcogenide Photocatalysts," *Journal of Physical Chemistry C* 117 (2013): 20440–20445, https://doi.org/10.1021/jp405808a.

249. S. Manzeli, D. Ovchinnikov, D. Pasquier, O. V. Yazyev, and A. Kis, "2D Transition Metal Dichalcogenides," *Nature Reviews Materials* 2 (2017): 17033, https://doi.org/10.1038/natrevmats.2017.33.

250. Y. Qiao, T. Hirtz, F. Wu, et al., "Fabricating Molybdenum Disulfide Memristors," *ACS Applied Electronic Materials* 2 (2020): 346–370, https://doi.org/10.1021/acsaelm.9b00655.

251. H. Li, C. Yoo, T. J. Ko, J. H. Kim, and Y. Jung, "Atomic-Scale Characterization of Structural Heterogeny in 2D TMD Layers," *Materials Advances* 3 (2022): 1401–1414, https://doi.org/10.1039/d1ma01013a.

252. C. Singh, M. A. Ali, V. Kumar, R. Ahmad, and G. Sumana, "Functionalized MoS2 Nanosheets Assembled Microfluidic Immunosensor for Highly Sensitive Detection of Food Pathogen," *Sensors and Actuators B: Chemical* 259 (2018): 1090–1098, https://doi.org/10.1016/j.snb.2017.12.094.

253. J. Qiu, P. Jiang, C. Wang, et al., "Lys-AuNPs@MoS2 Nanocomposite Self-Assembled Microfluidic Immunoassay Biochip for Ultrasensitive Detection of Multiplex Biomarkers for Cardiovascular Diseases," *Analytical Chemistry* 94 (2022): 4720–4728, https://doi.org/10.1021/acs.analchem.1c05061.

254. K. A. Novčić, C. Iffelsberger, S. Ng, and M. Pumera, "Local Electrochemical Activity of Transition Metal Dichalcogenides and Their Heterojunctions on 3D-Printed Nanocarbon Surfaces," *Nanoscale* 13 (2021): 5324–5332, https://doi.org/10.1039/d0nr06679f.

255. R. J. Toh, C. C. Mayorga-Martinez, J. Han, Z. Sofer, and M. Pumera, "Group 6 Layered Transition-Metal Dichalcogenides in Lab-On-a-Chip Devices: 1T-Phase WS2 for Microfluidics Non-Enzymatic Detection of Hydrogen Peroxide," *Analytical Chemistry* 89 (2017): 4978–4985, https://doi.org/10.1021/acs.analchem.7b00302.

256. X. Wang, C. Yang, M. Yan, and J. Yu, "A Sensitive Pb2+ Testing Method Based on Aptamer-Functionalized Peroxidase-Like 3D-Flower MoS2 Microspheres," *New Journal of Chemistry* 41 (2017): 7052–7060, https://doi.org/10.1039/c7nj00832e.

257. D. H. Ho, Y. Y. Choi, S. B. Jo, J. M. Myoung, and J. H. Cho, "Sensing with MXenes: Progress and Prospects," *Advanced Materials* 33 (2021): 2005846, https://doi.org/10.1002/adma.202005846.

258. B. Wang, W. Zhang, C. Lai, et al., "Facile Design of Flexible, Strong, and Highly Conductive MXene-Based Composite Films for Multifunctional Applications," *Small* 19 (2023): 2302335, https://doi.org/10.1002/smll.202302335.

259. X. Xiao, H. Wang, P. Urbankowski, and Y. Gogotsi, "Topochemical Synthesis of 2D Materials," *Chemical Society Reviews* 47 (2018): 8744–8765, https://doi.org/10.1039/c8cs00649k.

260. H. Tetik, J. Orangi, G. Yang, et al., "3D Printed MXene Aerogels With Truly 3D Macrostructure and Highly Engineered Microstructure for Enhanced Electrical and Electrochemical Performance," *Advanced Materials* 34 (2022): 2104980, https://doi.org/10.1002/adma.202104980.

261. M. Wan, A. Jimu, H. Yang, et al., "MXene Quantum Dots Enhanced 3D-Printed Electrochemical Sensor for the Highly Sensitive Detection of Dopamine," *Microchemical Journal* 184 (2023): 108180.

262. J. Zhang, R. Muñoz-Mármol, S. Fu, et al., "Interface-Tailored Secondary Excitation and Ultrafast Charge/Energy Transfer in Ti3C2Tx-MoS2 Heterostructure Films," *Journal of the American Chemical Society* 147 (2025): 10012–10022.

263. P. Xiao, G. Zhu, X. Shang, et al., "An Fe-MOF/MXene-Based Ultra-Sensitive Electrochemical Sensor for Arsenic(III) Measurement," *Journal of Electroanalytical Chemistry* 916 (2022): 116382.

264. M. Sharifuzzaman, A. Chhetry, M. A. Zahed, et al., "Smart Bandage With Integrated Multifunctional Sensors Based on MXene-Functionalized Porous Graphene Scaffold for Chronic Wound Care Management," *Biosensors and Bioelectronics* 169 (2020): 112637, https://doi.org/10.1016/j.bios.2020.112637.

265. J. B. M. Rocha Neto, J. C. Soares, G. A. Longhitano, et al., "Three-Dimensional Printing and Its Potential to Develop Sensors for Cancer With Improved Performance," *Biosensors-Basel* 12 (2022): 1.

266. X. Xu, C. Guan, L. Xu, et al., "Three Dimensionally Free-Formable Graphene Foam With Designed Structures for Energy and Environmental Applications," *ACS Nano* 14 (2020): 937–947, https://doi.org/10.1021/acsnano.9b08191.

267. M. Jo, S. Kim, G. Cho, T. M. Lee, J. Lee, and C. Lee, "Achieving Specified Geometric Quality in a Fully Printed Flexible Functional Layer Using Process Parameters in Roll-To-Roll Printed Electronics," *Flexible and Printed Electronics* 7 (2022): 14007, https://doi.org/10.1088/2058-8585/ac509a.

268. R. Abbel, P. Teunissen, E. Rubingh, et al., "Industrial-Scale Inkjet Printed Electronics Manufacturing—Production Up-Scaling From Concept Tools to a Roll-To-Roll Pilot Line," *Translational Materials Research* 1 (2014): 015002, https://doi.org/10.1088/2053-1613/1/015002.

269. T. R. Andersen, H. F. Dam, M. Hösel, et al., "Scalable, Ambient Atmosphere Roll-To-Roll Manufacture of Encapsulated Large Area, Flexible Organic Tandem Solar Cell Modules," *Energy and Environmental Science* 7 (2014): 2925–2933, https://doi.org/10.1039/c4ee01223b.

270. M. Bariya, Z. Shahpar, H. Park, et al., "Roll-To-Roll Gravure Printed Electrochemical Sensors for Wearable and Medical Devices," *ACS Nano* 12 (2018): 6978–6987, https://doi.org/10.1021/acsnano.8b02505.

271. T. Kothe, T. Maier, G. Mutinati, et al., "FLEPS 2022—IEEE International Conference on Flexible and Printable Sensors and Systems," (2022), Proceedings.

Biographies

Dr. Arshid Numan is an Associate Professor and Acting Head of the Sunway Center for Electrochemical Energy and Sustainable Technology (SCEEST), School of Engineering and Technology, Sunway University, Malaysia. He has 8 years of research experience developing 2D heterostructure nanomaterials for electrochemical energy storage and sensor applications. Dr. Numan has published over 150 high-impact research articles, edited 4 books and filed 4 patents. He was awarded the Sunway University Early Career Researcher Award for his excellence in research. He is also Listed in World's Top 2% Scientists in Energy and Materials by Stanford University, USA—Elsevier for 2021, 2022, and 2023. He has delivered more than two dozen invited talks, keynote and guest lectures at different international events.

Dr. Mohammad Khalid is a Professor in Materials for Green Energy Technologies at the University of Glasgow, UK. His research focuses on the synthesis of advanced nanomaterials for energy harvesting, storage and conversion applications. Dr. Khalid has authored over 400 peer-reviewed scientific articles, edited six books, and holds seven patents. In recognition of his contributions to materials science, he has been ranked among the top 2% of scientists globally since 2020. He is also a Fellow of the Higher Education Academy (FHEA), UK and the Royal Society of Chemistry (FRSC), UK.